INFLUENCE OF THE PRESENCE AND AMOUNT OF METAL NANOPARTICLES ON THE THERMAL AND MECHANICAL PROPERTIES OF iPP/SOFT PARAFFIN WAX PHASE CHANGE MATERIALS FOR THERMAL ENERGY STORAGE

by

MAMOHANOE PATRICIA MOLABA (B.Sc. Hons.)

Submitted in accordance with the requirements for the degree

MASTER OF SCIENCE (M.Sc.)

Department of Chemistry

Faculty of Natural and Agricultural Sciences

at the

UNIVERITY OF THE FREE STATE (QWAQWA CAMPUS)

SUPERVISOR: PROF A.S. LUYT

December 2014

DECLARATION

I declare that the thesis hereby submitted by me for the Master of Science degree at the University of the Free State is my own independent work and has not previously been submitted by me at another university/faculty. I furthermore cede copyright of the thesis in favour of the University of the Free State.

_____

Molaba M.P. (Ms)

DEDICATION

This is dedicated to my father (Diau Albert Molaba), mother (Dibabatso Esther Molaba), my late grandparents (Thoki Molaba, Mamothibedi Molaba, Hlakae Miya and Mapotlaki Miya) and my siblings (Rorisang Molaba and Mantshieng Molaba).

ABSTRACT

Nanocomposites based on iPP and an iPP/wax phase change blend with Ag nanoparticles were studied. The aim of this study was to correlate the thermal and electrical conductivity, as well as dynamic mechanical properties, with the morphology of the samples prepared using quenching in ice water and slow cooling from the melt, as well as different nanoparticle contents. Morphological analysis of the iPP/Ag nanocomposites showed that the Ag particles were well dispersed in the polymer, and formed nucleation centres for the crystallization of iPP. In the iPP/wax/Ag nanocomposites they were also well dispersed, but in the wax phase in between the iPP spherulites. The extent of filler agglomeration increased with increasing filler contents in both iPP and the iPP/wax blend. The Ag particles, whether in the iPP or wax phase, had little influence on the crystallinities and melting temperatures of iPP samples, even at higher filler contents. The presence Ag particles in iPP had little influence on the modulus of the iPP, but the presence of both wax and Ag particles significantly improved the modulus of these phase change nanocomposites. The thermal and electrical conductivities of the samples more significantly improved when both wax and Ag were present. With increasing Ag particle contents in both iPP/Ag and iPP/wax/Ag, the thermal conductivities increased, but leveled off at higher filler contents, while the electrical conductivities continuously increased with increasing filler contents. The slowly cooled samples had higher crystallinities than the quenched samples and therefore the slowly cooled samples were more thermally conductive than the quenched samples.

LIST OF ABBREVIATIONS

AC	Alternating current
CBED	Convergent beam electron diffraction
CF	Carbon fibre
CN	Carbon nanoparticles
CNF	Carbon nanofiber
CNT	Carbon nanotubes
CP	Carbon particles
DC	Direct current
DCP	Dicumyl peroxide
DMA	Dynamic mechanical analysis
DSC	Differential scanning calorimetry
EDS	Energy dispersive spectroscopy
EELS	Electron energy loss spectroscopy
EG	Expanded graphite
GnP	Graphene nanoplatelet
GnPs	Graphite nanoplatelets
GNs	Graphene nanosheets
HDPE	High density polyethylene
HDPE-EVA	High-density poly(ethylene-ethylene vinyl acetate)
HNT	Halloysite nanotubes
iPP	Isotactic polypropylene
LDPE	Low-density polyethylene
LLDPE	Linear low-density polyethylene
$mSiO_2$	Modified silica
MWCNT	Multiwalled carbon nantubes
OMT	Organophilic montmorillonite
PCM	Phase change material
PEG	Poly(ethylene glycol)
PMMA	Poly(methyl methacrylate)

PS	Polystyrene
PVDF	Poly(vinylidene difluoride)
rGO	Reduced graphene oxide
SBS	Styrene-butadiene-styrene
SEBS	Styrene-ethylene-butadiene-styrene
SEM	Scanning electron microscopy
TEM	Transmission electron microscopy

TABLE OF CONTENTS

LIST OF TABLES

LIST OF FIGURES

CHAPTER 1

Introduction and literature review

1.1 Introduction

The gap between energy supply and demand can be eliminated by the use of proper energy storage methods [1]. There are different energy storage methods, i.e. electrical, mechanical and thermal energy storage. In electrical energy storage, energy is stored in batteries. A battery is charged by connecting it to a source of direct current and when it is charged, the stored chemical energy is converted into electrical energy. Mechanical energy storage involves gravitational energy storage or pumped hydropower storage. Storage of energy is carried out when inexpensive off peak power is available, i.e. at night and weekends [2]. Thermal energy storage is achieved by cooling, heating, melting, solidifying, or vaporizing a material with the energy becoming available as heat when the process is reversed [3].

Among the mentioned energy storage methods, thermal energy has gained great interest. This is due to its storing and releasing ability [2]. There are different ways in which thermal energy can be stored i.e. thermomechanical, sensible and latent heat energy storage. Thermomechanical energy storage is based on the energy absorbed and released in breaking and reforming molecular bonds. In this case thermal energy depends on the storage capacity of the material, the endothermic heat of reaction and the extent of conversion. In sensible heat storage, thermal energy is stored by increasing the temperature of a solid or liquid without changing phase. The amount of the absorbed thermal energy in sensible heat depends on the specific heat of the medium, the temperature change and the storage capacity of the material. In latent heat storage, thermal energy is absorbed or released when a material changes phase from solid to liquid or liquid to solid [2,5,6].

Latent heat is an attractive thermal energy storage method. This is due to its storing and releasing of a large amount of energy per weight of a material at constant temperature [7-9]. Typical latent heat storage materials are phase change materials (PCMs). PCMs are substances that are capable

of storing and releasing energy; they can undergo a solid-liquid, liquid-solid, solid-gas and liquid-gas phase change over a narrow temperature range [10,11]. The solid-liquid and liquid-solid systems are the most preferred systems because they store a fairly large quantity of heat over a narrow temperature range, with small volume change, whereas the solid-gas and liquid-gas occupies large volumes which makes the system complex and difficult to handle [2,9,12-14]. PCMs are used as latent heat thermal energy storage media, in areas of passive and active storage systems, heating or cooling of water, solar energy storage, electronics, automotive industry, food industry, biomaterial and biomedical applications [3].

PCMs are classified into three main categories. These are eutectics, inorganics and organics. Eutectics involve organics and inorganics with high volumetric storage densities. Inorganic PCMs include salt hydrates, salts, metals, and alloys. They generally have high volumetric latent heat storage capacity which is twice those of organic PCMs. However, their utility is limited due to their non-uniform melting and supercooling effects. Organic PCMs involve fatty acids and paraffins [15,16]. They melt and freeze continually without phase segregation and a decrease in their latent heat of fusion [3]. Amongst the above mentioned organic PCMs, paraffins have gained great interest due to their promising properties. They are more chemically stable than inorganic substances, have high latent heat of fusion, are commercially available at reasonable cost and exhibit little or no supercooling [17-19].

Paraffins are mixtures of hydrocarbons, characterized by straight or branched carbon chains with the general formula C_nH_{2n+2} [20]. They are produced from crude oil and the Fischer-Tropsch process [21]. Paraffin waxes crystallize in layers that consist of molecules having zigzag conformations [22]. They are used in the production of candles, paper coating, protective sealant for food products and beverages, glass-cleaning preparations, floor polishing and stoppers for acid bottles [23]. Paraffin waxes are combustible and have good dielectric properties. However, when used as PCMs, paraffin waxes need a supporting material to prevent their leakage during the phase change process.

There are two methods that can be used to prevent leakage of the phase change materials. These are blending and encapsulation of paraffin wax with polymers. The encapsulated PCM is

composed of the PCM as the core and a polymer shell to maintain the shape and to prevent leakage of the PCM during a phase change process [24,25]. In blending, the polymer fixes the PCM in a compact shape during the phase change process, and hence prevent leakage [26]. However, if polyolefins are used as the fixing polymers, both the polymer and the paraffin wax have low thermal conductivity which results in a slow heat transfer [27,28].

There are different techniques used to improve the thermal conductivity of the form-stable PCMs. This includes the introduction of conductive micro- and nano-fillers [29]. The addition of nano-particles is the preferred method for improving the thermal conductivity of PCMs because they offer improved properties at relatively low filler content due to their large surface areas [1]. Conductive nano-fillers used for thermal conductivity enhancement includes aluminum, silver, copper, graphite and carbon black powders [29]. For this work we chose silver because it has very good electrical and thermal conductivities [30].

1.2 Literature review

1.2.1 Polymer/wax blends

A number of studies have been conducted on blending of paraffin wax with polyolefins [7,11,23,25,31-38]. The blends were prepared using a variety of processing techniques such as melt mixing, melt extrusion, in situ polymerization and mechanical methods. Among all the aforementioned methods melt mixing is the most commonly used technique because it is cheaper, easier and not time consuming. In all these studies, different grades of paraffin wax with different melting temperatures were used. This includes technical grade, soft, hard and oxidised paraffin wax. Different morphologies were observed for different grades of paraffin wax blended with polyolefins. For example, in the system of an HDPE/wax blend the authors reported that paraffin wax was well dispersed in the network structure of HDPE. This was an indication that HDPE kept paraffin in a compact shape to prevent its leakage [31-33]. It was also reported that the blends containing equal concentrations of HDPE and wax showed no difference in morphology. This was attributed to the similar chemical structures of HDPE and paraffin wax [7].

Blending of soft and hard paraffin wax with polypropylene (PP) and low density polyethylene (LDPE) was reported in a few studies [11,34,35]. In these studies the authors generally observed two-phase morphology of the blends. The blends based on hard and soft paraffin waxes showed different morphologies. Apparently that soft paraffin wax, because of its lower molar mass and viscosity, could separate more easily from the polymers than the hard paraffin wax. Different morphologies were observed when increasing the wax content in LLDPE/wax blends [35]. It was reported that an increase in wax content caused the blends to rupture along different lines.

The immiscibility of the components in polymer/wax blends was confirmed by a number of studies based on the reported thermal properties [7,11,20,23,25,34-36,37,38]. In these studies, polyolefins were blended with different grades of paraffin wax. The blends were prepared using a variety of processing techniques such as melt mixing, melt extrusion and mechanical methods. In these studies, different types of behaviour were observed depending on the method and the type of wax used. The authors observed a general decrease in the melting temperatures of the polymer matrix and this was attributed to the plasticizing effect of the wax. It has also been reported that the melting enthalpies of the blends increased with wax loading [11,23,25,34-36,37,38]. This increase was attributed to the contribution of the highly crystalline wax. It is well known that the melting enthalpy is directly related to the crystallinity [37,39-42].

The thermal properties of PP/wax blends were investigated for the creation of shape stabilized phase change materials [11,36]. In this study isotactic polypropylene (PP) was blended with soft and hard Fischer-Tropsch paraffin waxes. It was observed that the specific melting enthalpy related to the wax portion increased with an increase in wax content, while the melting enthalpy related to the PP portion decreased. The thermal behaviour of refined and semi-refined wax blended with high-density polyethylene (HDPE) was reported in another study [7], where multiple peaks corresponding to wax and HDPE were observed for the form stable blends.

A single endothermic peak was observed in the DSC curves of LLDPE/hard paraffin wax blends at low wax loadings [23], while LLDPE/soft paraffin wax blends showed two separate melting peaks for all the blends with different wax loadings [25]. It was concluded that the hard paraffin wax and LLDPE were miscible in the crystalline phase, whereas soft paraffin wax was

immiscible with the matrix for all the investigated wax loadings. Similar studies were done on the thermal behaviour of wax blended with LDPE [34,38]. A single endothermic peak was reported at low wax contents in the case of the LDPE/hard wax blends [38], which was attributed to the miscibility and co-crystallization of the wax and LDPE. However, in the case of LDPE/soft wax blends, multiple peaks were observed for the different wax loadings [34]. A decrease in the melting temperature of LDPE and LLDPE in the blends with an increase in wax loading was also reported [25,34]. This was attributed to the formation of smaller crystallites due to the miscibility of the components in the molten state and the plasticizing effect of the wax. The authors reported that soft paraffin wax has strong London interactions with LDPE as a result of the miscibility in the melt, and their effect on the melting of LDPE was more significant. In the case of HDPE, the authors observed two melting peaks when blending with hard and soft paraffin waxes. The peak that appeared at lower temperatures was related to the melting of wax crystals, whereas the peak at higher temperatures was related to the melting of the polyolefin crystals. The observed separate melting peaks of the blends were reported to be an indication of the immiscibility of the blends as confirmed by morphology studies [25,37].

A limited amount of research was done on the crosslinking of polymer/wax blends [23,38]. Different behaviour was observed when uncrosslinked and crosslinked LLDPE/hard paraffin wax blends were investigated [23]. The melting temperature of uncrosslinked LLDPE remained unchanged in the presence of hard paraffin wax, while in the presence of a crosslinking agent, a decrease in the melting temperature and an increase in the melting enthalpy with the addition of DCP was observed [23]. The authors concluded that the presence of a crosslinking agent reduced the crystallinity of the polyolefins. However, the study on LDPE/hard paraffin wax attributed the decrease in melting temperature to a reduction in the lamellar thickness of the crystallites [38]. In this study the melting enthalpies of the blends also increased with an increase in wax content as a result of an increase in crystallinity.

A number of studies investigated the thermomechanical properties of polyolefin/paraffin wax blends [11,34,37,43-45]. In these studies, different behaviour was observed for the different grades of paraffin wax used. The authors reported mostly on the effect of wax on the storage modulus and loss tangent of the polymer. It was generally observed that the storage modulus

increased at temperatures below the melting of wax, and decreased above it. It was concluded that hard paraffin wax in its solid state reinforced the polymer, whereas soft paraffin wax acted as a highly crystalline filler which immobilized the polymer chains at the crystal surface. Similar results were reported on HDPE/soft paraffin blends [37]. These authors also reported higher and lower temperature relaxation peaks corresponding to HDPE and the wax.

In the PP/soft paraffin wax blends, a decrease in the storage modulus was observed with an increase in wax loading [11,43]. This was attributed to the plasticizing effect of the PP matrix by the wax. Three relaxation peaks, corresponding to the solid-solid transition in wax, and the melting of the wax and PP, were observed [11]. In the case of PP/polystyrene (PS):wax microcapsules, the blends showed three relaxation peaks in the presence and absence SEBS [43]. The β relaxation, which is usually related to the glass transition temperature of PP, was observed at lower temperatures for the blends. A transition corresponding to the melting of wax was also observed in the temperature range 40-60 °C, whereas the relaxation corresponding to the glass transition of PS appeared at higher temperatures. The glass transition of PP in the blends shifted to lower temperatures compared to that of the pure polymer. This was attributed to the increase in free volume of PP in the presence of the paraffin wax microcapsules. The presence of the SEBS modifier had no influence on these properties. It formed a layer around the microcapsules without affecting the interaction between PP and the microcapsules.

In the case of an HDPE matrix blended with hard and soft paraffin wax, pure HDPE showed a high storage modulus and no specific trends were reported with an increase in wax loading [44,45]. The lower storage modulus of the blends indicated a plasticizing effect of the wax. In these studies two relaxation peaks corresponding to α- and γ-transitions were observed. The γ-relaxation remained the same with an increase in wax content, while the α-relaxation shifted to lower temperatures. The decrease in the temperature of the α-relaxation was attributed to thinner lamellae. An additional peak related to the β-relaxation of HDPE was observed at higher wax loadings [44].

1.2.2 Polymer/wax blend composites

The morphologies of form-stable PCM composites were investigated in a number of studies using scanning electron microscopy (SEM) [44-50]. Different morphologies were reported depending on the method used to prepare the samples. The polymer/wax blends were mixed with different fillers such as wood-flour, copper, and clay. Generally the authors observed two phase morphologies with the filler covered by wax. This was attributed to a higher affinity between the fillers and the wax, the separate crystallization of wax in the amorphous phase of the polymer, and to the thermodynamically more preferred adsorption of the smaller wax molecules onto the rough filler surfaces.

In studies on HDPE-EVA alloy/wax/organophilic montmorillonite (OMT) [47,48] the authors reported that the wax was dispersed in the three-dimensional network structure formed by HDPE-EVA. This was attributed to the fact that paraffin wax and HDPE have similar structures, and thus could be easily mixed with polyethylene. The OMT filler particles apparently acted as interfacial modifiers which improved the dispersion of the blend components. Similar studies on the morphology of PMMA/PEG and their composites prepared through *in situ* polymerization showed good dispersion of the filler particles [49,50], and of PEG in the network structure of PMMA. The filler particles were also well dispersed in the blends.

The latter studies [49,50] also investigated the melting behaviour of form-stable PCM composites. The composites showed two endothermic peaks corresponding to the melting of wax and the polymer crystals. This was attributed to the immiscibility of wax and polymer in the composites. Other authors [46] reported that in the PE/soft paraffin wax system the presence, type and amount of the filler particles did not change the melting temperatures of PE or wax in the composites. However, in the case of HDPE/soft paraffin wax/wood flour composites a decrease in the melting temperatures of the HDPE in the composites was observed with an increase in wax content at a specific filler content [45]. This was attributed to the plasticizing effect of wax.

The studies on HDPE-EVA/wax/OMT [47,48] reported two melting peaks for both the pure paraffin and the form-stable PCM composites. This was an indication that there was no chemical reaction between the paraffin, HDPE-EVA and the organophilic montmorillonite (OMT) during composite preparation. The phase change peaks of the form stable PCM composites were less intense compared to that of the pure paraffin. This was because the three-dimensional net structure, observed in the morphology studies, confined the heat movement to and from the paraffin during the phase change. The latent heat of the form stable PCM composites decreased with an increase in OMT loadings [47,48]. In the case of PMMA/PEG form-stable composites incorporated with graphite nanoplatelets (GnPs) and aluminum nitride (AlN), the authors reported insignificant changes in the melting temperatures of the composites [49,50]. The melting enthalpy of the composites increased with an increase in PEG content [49], but in the case of PMMA/PEG/GnP the authors observed a decrease in the melting enthalpy of the PCM in the composites [50].

There were a limited number of studies on the thermomechanical properties of form-stable PCM composites [45,51]. In these studies graphite and wood flour were incorporated in the form-stable PCM blends. An increase in storage modulus was observed with an increase in filler content in the case of LDPE/soft paraffin wax/graphite [51], which was explained as being an indication that graphite reinforced the matrix and countered the softening effect of the wax. The glass transition temperature of these composites also increased and broadened with an increase in filler content. This was attributed to the immobilization of the polymer chains by the wax and the filler particles in the amorphous phase of the polyolefin matrix. In the case of HDPE/soft paraffin wax/wood flour [45] no specific trends related to the amount of filler particles were observed. However, the presence of the filler particles in the polymer/wax blends reduced the storage modulus and induced a shift in both the γ- and α- transitions towards higher temperatures. This was related to the restricted motions of the polymer chains and the increased lamellar thickness with the addition of filler particles.

A number of studies investigated the thermal conductivity of form-stable PCM composites [27,33,46,50,51]. The form-stable PCMs used in all the studies were based on different grades of paraffin wax blended with polymers. Graphite and copper were incorporated in the PCM blends

to improve the thermal conductivity. The authors reported a general increase in thermal conductivity of the composites with an increase in filler content. Moreover, a significant increase in thermal conductivity was reported in the case of the composites incorporated with expanded graphite [33,51]. This was attributed to a better dispersion of expanded graphite in the presence of wax in the blends. However, the thermal conductivity of PE/soft paraffin wax/Cu composites initially decreased at low filler content and increased at higher filler loadings [46]. The initial decrease was reported to be the result of the voids formed at the interface between the polymer and the wax. In the case of PMMA/PEG/GnP composites an increase in thermal conductivity with an increase in filler content was also observed [50], as well as the formation of thermally conductive paths at higher filler loadings.

Some authors studied the effect of the preparation method on the thermal conductivity of shape stabilized paraffin/SBS/EG composites [27]. In this study two different methods were used to prepare the composites. In the first method the EG, paraffin and SBS were mixed on a two roll mill, while in the second method EG was directly added to the molten paraffin/SBS shape stabilized blends. There was an increase in the heat transfer for both the solidification and heating processes with the addition of EG. However, a faster heat transfer was reported for the composites prepared using the second method. This was attributed to the formation of a thermally conductive network.

1.2.3 Polymer/filler composites

The morphology of polymers incorporated with different fillers was investigated in a number of studies [52-57]. The polymer composites were prepared using methods such as melt mixing method and *in situ* polymerization. Different behaviour was observed depending on the size and type of filler used. In HDPE/Ag nanocomposites the Ag nanoparticles were in contact with one another, and this was attributed to the large surface areas of the nanoparticles. The silver nanoparticles had a tendency to form agglomerates, especially when the composites were prepared using melt mixing [56]. However, in LDPE/Cu nano and micro composites [57] the copper micro particles were well dispersed with no obvious agglomeration, while the copper nanoparticles were fairly dispersed with obvious agglomerations.

The morphology of different fillers such as carbon nanoparticles (CN), fumed silica and nanosilica in PP where the composites were prepared through melt mixing, was investigated in a few studies [52-55]. In the case of PP/CN the filler particles were well dispersed as individual particles at low filler content [52,54]. However, at higher filler loadings filler agglomerations were observed with a reduction in the number of individual particles. This was attributed to the higher surface energy of the nanoparticles and the presence of reactive functional groups which caused stronger interaction between the particles and the formation of large aggregates. However, when fumed silica and nanosilica were used, filler agglomerations were observed at all filler contents indicating poor interaction between the filler and the polymer [53,55]. The sizes of the aggregates depended on the filler content, with larger aggregates at higher filler loadings. Even when compatibilizers were used to improve the interaction and dispersion of the fillers in the matrix, there were still aggregates, but they were smaller. In the case of PP/nanosilica [55], silane-treated mSiO_2 was dispersed more effectively than unmodified SiO_2. This was attributed to the increase in affinity of the modified filler to the polymer because of the compatibilizer. Acid treatment of the filler particles was also used to improve the dispersion of multiwalled-carbon nanotubes (MWCNT) in PP [58], and a decrease in size of the aggregates was reported. The acid oxidation treatment was reported as a cutting process for filler particles by reducing the length and entanglements of the fillers.

A number of studies investigated the thermal properties of polymer/filler composites [56,57]. Generally there was a decrease in melting enthalpy of the polymer with increase in filler content. There were, however, no significant changes in the melting temperatures of the polymers with the addition of fillers. A decrease in the melting enthalpies was reported in the case of polyethylenes incorporated with both micro- and nano-sized copper. This was attributed to a reduction in chain mobility which gave rise to the lower crystallinity. In the case of HDPE/Ag nanocomposites [56] an increase in crystallization temperatures of the composites was observed, indicating that the Ag nanoparticles acted as nucleation sites for the polymers.

The melting and crystallization behaviour of PP incorporated with different filler particles such as silver (Ag) and graphene nanosheets (GNs), exfoliated graphene and carbon nanofiber (CNF) were investigated in a number of studies [39-41,59-61]. Different methods such as melt

extrusion, melt compounding, facile solution dispersion and melt mixing were used to prepare the composites. In all these studies, the nanocomposites showed either one [39,41,42] or two melting peaks [40,59,61]. However, in the case of PP/GNs composites two melting peaks were observed for pure PP while the composites showed one melting peak [60]. The two melting peaks were attributed to the melting of both α-crystals at higher temperatures and β-crystals at lower temperatures [59]. The α-phase is the thermodynamically stable crystalline form of PP and appears under normal processing conditions, while the β-phase is a thermodynamically unstable phase which is usually observed in commercial grades of PP at higher undercooling. This phase can also be generated under some specific conditions, such as quenching, and hence it is not observed in some of the PP composites [62,63]. In PP/Ag nanocomposites based on the organic-soluble Ag nanocrystals and pure Ag nanoparticles very similar behaviour was reported [40,59], although there were observable differences. When organic-soluble Ag nanocrystals, that were coated with a mono-layer of surfactants consisting of oleic acid and alkylamine, were incorporated in PP, an increase in the intensity of the β-peak and a decrease in the intensity of the α-peak were observed [40]. Apparently the organic-soluble Ag nanocrystals promoted the nucleation and crystallization of β-crystals during quiescent conditions. However, when pure Ag nanoparticles were used, the intensity of the α-peak remained fairly constant while a β-peak started developing and increased in intensity with increasing nanofiller content [59]. Negligible changes in the melting behaviour of PP composites were reported with the addition of EG, CNF and Ag nanoparticles and with increasing filler content [41,42,61], while in the case of PP/GNs the melting temperature increased [60]. An increase in the crystallization temperatures of the PP composites with an increase in EG and Ag content was observed [41,59,61]. This was attributed to the filler particles acting as nucleating sites for PP.

When copper particles were incorporated in polyethylenes [57], the storage modulus of the composites increased with an increase in filler content. This was attributed to the stiffening effect of the filler particles on the polymer matrix. Different relaxations were reported for the different polyethylenes. In case of LDPE and LLDPE, three relaxations were observed in the order of increasing temperature, i.e. γ-, β-, and α-transitions. However, in the case of HDPE two relaxations were reported, i.e. γ- and α-transitions. The β-transition which corresponds to the glass transition temperature was difficult to identify in the highly crystalline HDPE matrix.

The effect of different fillers such as carbon black, carbon particles (CP) and carbon fibre (CF), graphene nanosheets (GNS), wollastonite, attapulgite and halloysite on the thermomechanical properties of PP were studied [52,64-68]. In all these studies the storage modulus of the composites increased with an increase in filler content. The presence of the fillers in the polymer strengthened the matrix by reducing the deformation of the matrix and the mobility of the chains. In the PP/GNS system the composites showed three relaxations in the tan δ curves, namely α, β and γ in the order of increasing temperature [65]. In the case of PP/wollastonite composites, two relaxations, γ and β, were observed [66]. Further additions of the filler particles led to an increase in the intensity of the β-relaxation. However, depending on the temperature range in which the viscoelastic properties were studied, some of the relaxations were not observed in the composites [52,64,67,68]. The β-relaxation, which is usually associated with the motions within the amorphous regions, shifted to higher temperatures with an increase in filler contents. This was attributed to a reduction in the macromolecular chain mobility of the polymer due to the strong interaction with the filler particles. However, in the case of PP/halloysite nanotubes (HNT) nanocomposites, the glass transition temperature of the composites decreased with the addition of the filler particles [68]. This was attributed to the poor interfacial adhesion between the HNTs and the PP matrix. Apparently the incorporation of filler particles deteriorated the entanglement and interaction among PP molecules by mobilizing the polymer chains, which led to a decrease in T_g. Surface modification of the filler particles led to an increase in T_g with an increase in filler content. This was attributed to the improved interfacial adhesion between the matrix and the filler particles, reducing the mobility of the PP chains.

In studies on the thermal conductivity of polymer/filler composites, [56,57,69] an increase in the thermal conductivity was generally observed. This increase was attributed to a number of factors such as the crystallinity of the polymer and the high thermal conductivity of the filler. Higher thermal conductivity values were reported for HDPE because of the higher degree of crystallinity of this polymer. In the case of HDPE/Ag [56] and PVDF/Ag [69] composites, an increase in thermal conductivity with an increase in filler content was observed. This was attributed to the formation of the thermally conductive paths at higher filler contents.

A number of studies showed that polypropylene was commonly studied in the formation of conductive polymer composites [64,70-72]. The effect of different conductive fillers such as graphite, graphene, carbon nanotubes (CNT), Al-flake, CP and CF on the thermal conductivity of polypropylene composites was investigated. In these studies graphite particles of up to 20 wt%, graphene up to 5 wt%, CP and CF up to 40 wt%, CNT up to 5 wt% and Al-flake up to 50 wt% were incorporated in polypropylene. The composites were prepared using melt mixing and melt extrusion. The thermal conductivity always increased with an increase in filler content, especially at higher loadings. Despite the weak interaction of PP and Al-flake, the PP/Al-flake composites showed the highest thermal conductivity [72], probably because of the higher Al-flake content used. PP/CP showed the lowest thermal conductivity, which was attributed to the agglomeration of the carbon particles [64].

In a study on the electrical conductivity of HDPE/Ag composites prepared through melt extrusion, a linear dependence of AC conductivity on frequency was reported at lower filler loadings, which indicated an insulating behavior [56]. For higher filler loadings, a DC plateau region was observed, which indicated conductive behaviour of the composites. The dielectric properties of PP filled with various conductive fillers such as multiwalled carbon nanotubes (MWCNTs), carbon nanofibre (CNF), graphene, and reduced graphene oxide (rGO), prepared through a variety of methods, were also investigated [73-79]. Generally, the composites showed two different types of behaviour depending on the filler content. The AC conductivity of pure PP and the composites with low filler content increased linearly with frequency. This is typical behaviour for insulating materials, indicating that the electrical properties of the composites are controlled by the matrix. At this concentration the conductive particles are too far apart to allow electrical conduction. At high filler loadings the conductivity showed a DC plateau accompanied by a significant increase in conductivity. In this case the electrical conductivities of the composites were independent of the frequency, indicating the formation of three-dimensional interconnecting networks by the dispersed fillers. This is typical behaviour for electrically conductive materials, indicating that the electrical properties of the composites are controlled by the conductive fillers. The PP/rGO composites showed a lower electrical percolation threshold [76]. The influence of surface modified and as prepared filler particles on the electrical conductivities of PP/MWCNTs nanocomposites was compared [78]. The authors reported higher

conductivity with lower percolation threshold for the composites with surface modified filler particles. A similar investigation was done on PP incorporated with sonicated and pristine graphene nanoplatelets (GnP) [79]. In the case of the sonicated filler particles, lower conductivity with a much higher percolation was reported. This was attributed to a reduction in the size of filler aggregates and a uniform distribution of filler particles in the polymer matrix.

1.3 Aims and objectives

The main aim of this study was to correlate the thermal and electrical conductivity with the morphology of the samples prepared using different conditions. These conditions were quenching in ice water and slow cooling from the melt. iPP/wax blends at different wax ratios, iPP/Ag nanocomposites at different Ag loadings and iPP/wax/Ag shape-stabilized PCM nanocomposites were prepared. The dispersion of Ag particles in iPP and iPP/wax blend, the influence of different Ag contents, and the influence of quenching and slow cooling treatments on the morphology, thermal and dynamic mechanical properties, and the thermal and electrical conductivities were investigated. All the investigated properties were explained in terms of the obtained morphologies.

1.4 Thesis outline

- Chapter 1: Introduction and literature survey
- Chapter 2: Materials and methods
- Chapter 3: Results and discussion
- Chapter 4: Conclusions

1.5 References

[1] A. Sari, A. Karaipekli. Thermal conductivity and latent heat thermal energy storage characteristics of paraffin/expanded graphite composite as phase change material. Applied Thermal Engineering 2007; 27:1271-1277.
DOI: 10.1016/j.applthermaleng.2006.11.004

[2] A. Sharma, V.V. Tyagi, C.R. Chen, D. Buddhi. Review on thermal energy storage with phase change materials and applications. Renewable and Sustainable Energy Reviews 2009; 13:318-345.
DOI: 10.1016/J.RSER.2007.10.005

[3] K. Pielichowska, K. Pielichowski. Phase change materials for thermal energy storage. Progress in Materials Science 2014; 65:67-123.
DOI: 10.1016/j.pmatsci.2014.03.005

[4] B. He, F. Setterwall. Technical grade paraffin waxes as phase change materials for cool thermal storage and cool storage systems capital cost estimation. Energy Conversion and Management 2002; 43:1709-1723.
DOI: 10.1016/S0196-8904(01)00005-X

[5] M.M. Farid, A.M. Khudhair, S.A.K. Razack, S. Al-Hallaj. A review on phase change energy storage: Materials and applications. Energy Conversion and Management 2004; 45:1597-1615.
DOI:10.1016/j.enconman.2003.09.015

[6] S.M. Hasnain. Review on sustainable thermal energy storage technologies. Part 1: Heat storage materials and techniques. Energy Conversation and Management 1998; 39:1127-1138.
DOI: 10.1016/SO196-8904(98)00025-9

[7] Y. Hong, G. Xin-shi. Preparation of polyethylene-paraffin compound as a form-stable solid-liquid phase change material. Solar Energy Materials & Solar Cells 2000; 64:37-44.
DOI: 10.1016/S0927-0248(00)00041-6

[8] X. Xiao, P. Zhang. Morphologies and thermal characterization of paraffin/carbon foam composite phase change material. Solar Energy Materials & Solar Cells 2013; 117:451-461.
DOI: 10.1016/j.solmat.2013.06.037

[9] C. Alkan, A. Sari. Fatty acid/poly(methyl methacrylate) (PMMA) blends as form-stable phase change materials for latent heat thermal energy storage. Solar Energy 2008; 82:118-124.
DOI: 10.1016/j.solener.2007.07.001

[10] A. Koca, H.F. Oztop, T. Koyun, Y. Varol. Energy and exergy analysis of a latent heat storage system with phase change material for a solar collector. Renewable Energy 2008; 33:567-574.
DOI: 10.1016/j.renene.2007.03.012

[11] I. Krupa, G. Miková, A.S. Luyt. Polypropylene as a potential matrix for the creation of shape stabilized phase change materials. European Polymer Journal 2007; 43:895–907.
DOI: 10.1016/j.eurpolymj.2006.12.019

[12] N. Sarier, E. Onder. Organic phase change materials and their textile applications: An overview. Thermochimica Acta 2012; 540:7-60.
DOI: 10.1016/j.tca.2012.04.013

[13] A.F. Regin, S.C. Solanki, J.S. Saini. Heat transfer characteristics of the storage system using PCM capsules: A review. Renewable and Sustainable Energy Reviews 2008; 12:2438-2458.
DOI:10.1016/j.rser.2007.06.009

[14] H.S. Fath. Technical assessment of solar thermal energy storage technologies. Renewable Energy 1998; 14:35-40.
DOI: 10.016/SO960-1481(98)00044-5

[15] A. Pasupathy, R. Velraj, R.V. Seeniraj. Phase change material-based building architecture for thermal management in residential and commercial establishments. Renewable and Sustainable Energy Reviews 2008; 12:39-64.
DOI: 10.1016/j.rser.2006.05.010

[16] J.N. Shi, M.D. Ger, Y.M. Liu, Y.C. Fan, N.T. Wen, C.K. Lin, N.W. Pu. Improving the thermal conductivity and shape-stabilization of phase change materials using nanographite additives. Carbon 2013; 51:365-372.
DOI: 10.1016/j.carbon.2012.08.068

[17] K. Zhang, B. Han, X. Yu. Electrically conductive carbon nanofiber/paraffin wax composites for electric thermal storage. Energy Conversion and Management 2012; 64:62-67.
DOI: 10.1016/j.enconman.2012.06.021

[18] S. Kim, L.T. Drzal. High latent storage and high thermal conductive phase change materials using exfoliated graphite nanoplatelets. Solar Energy Materials and Solar Cells 2009; 93:136-142.
DOI: 10.1016/j.solmat.2008.09.010

[19] J. Xiang, L.T. Drzal. Investigation of exfoliated graphite nanoplatelets (xGnP) in improving thermal conductivity of paraffin wax-based phase change material. Solar Energy Materials and Solar Cells 2011; 95:1811-1818.
DOI: 10.1016/j.solmat.2011.01.048

[20] I. Krupa, A.S. Luyt. Physical properties of blends of LLDPE and an oxidized paraffin wax. Polymer 2001; 42:7285-7289.
DOI: 10.1016/S0032-3861(01)00172-0

[21] J.C. Crause, I. Nieuwoudt. Paraffin wax fractionation: State of the art vs. supercritical fluid fractionation. Journal of Supercritical Fluids 2003; 27:39-54.
DOI: 10.1016/S0896-8446(02)00185-7

[22] M. Zbik, R.G. Horn, N. Shaw. AFM study of paraffin wax surfaces. Colloids and Surfaces A: Physicochemical Engineering Aspects 2006; 287:139-146.
DOI:10.1016/j.colsurfa.2006.03.043

[23] I. Krupa, A.S. Luyt. Thermal properties of uncross-linked and cross-linked LLDPE/wax blends. Polymer Degradation and Stability 2000; 70:111-117.
DOI: 10.1016/S0141-3910(00)00097-5

[24] G. Fang, Z. Chen, H. Li. Synthesis and properties of microencapsulated paraffin composites with SiO_2 shell as thermal energy storage materials. Chemical Engineering Journal 2010; 163:154-159.
DOI: 10.1016/j.cej.2010.07.054

[25] J.A. Molefi, A.S. Luyt, I. Krupa. Comparison of LDPE, LLDPE and HDPE as matrices for phase change materials based on a soft Fischer–Tropsch paraffin wax. Thermochimica Acta 2010; 500:88-92.
DOI: 10.1016/j.tca.2010.01.002

[26] C. Koning, M. Van Duin, C. Pagnoulle, R. Jerome. Strategies for compatibilization of polymer blends. Progress in Polymer Science 1998; 23:707-757.
DOI: 10.1016/S0079-6700(97)00054-3

[27] M. Xiao, B. Feng, K. Gong. Preparation and performance of shape stabilized phase change thermal storage materials with high thermal conductivity. Energy Conversion and Management 2002; 43:103-108.
DOI: 10.1016/S0196-8904(01)00010-3

[28] A. Mills, M. Farid, J.R. Selman, S. Al-Halla. Thermal conductivity enhancement of phase change materials using a graphite matrix. Applied Thermal Engineering 2006; 26:1652-1661.
DOI: 10.1016/j.applthermaleng.2005.11.022

[29] D. Fernandes, F. Pitié, G. Cáceres, J. Baeyens. Thermal energy storage: "How previous findings determine current research priorities". Energy 2012; 39:246-257.
DOI: 10.1016/j.energy.2012.01.024

[30] A. Tadjarodi, F. Zabihi. Thermal conductivity studies of novel nanofluids based on metallic silver decorated mesoporous silica nanoparticles. Materials Research Bulletin 2013; 48:4150-4156.
DOI: 10.1016/j.materresbull.2013.06.043

[31] Y. Cai, Y. Hu, L. Song, Y. Tang, R. Yang, Y. Zhang, Z. Chen, W. Fan. Flammability and thermal properties of high density polyethylene/paraffin hybrid as a form-stable phase change material. Journal of Applied Polymer Science 2006; 99:1320-1327.
DOI: 10.1002/app.22065

[32] H. Inaba, P. Tu. Evaluation of thermophysical characteristics on shape-stabilized paraffin as a solid-liquid phase change material. Heat and Mass Transfer 1997; 32:307-312.
DOI: 10.1007/s002310050126

[33] A. Sari. Form-stable paraffin/high density polyethylene composites as solid–liquid phase change material for thermal energy storage: Preparation and thermal properties. Energy Conversion and Management 2004; 45:2033-2042.
DOI: 10.1016/j.enconman.2003.10.022

[34] I. Krupa, G. Miková, A.S. Luyt. Phase change materials based on low-density polyethylene/paraffin wax blends. European Polymer Journal 2007; 43:4695-4705.
DOI: 10.1016/j.eurpolymj.2007.08.022.

[35] I. Krupa, A.S. Luyt. Thermal and mechanical properties of extruded LLDPE/wax blends. Polymer Degradation and Stability 2001; 73:157-161.

DOI: 10.1016/S0141-3910(01)00082-9

[36] I. Krupa, A.S. Luyt. Thermal properties of polypropylene/wax blends. ThermochimicaActa 2001; 372:137-141.
DOI: 10.1016/s0040-6031(01)00450-6

[37] M.E. Sotomayor, I. Krupa, A. Várez, B. Levenfeld. Thermal and mechanical characterization of injection moulded high density polyethylene/paraffin wax blends as phase change materials. Renewable Energy 2014; 68:140-145.
DOI: 10.1016/j.renene.2014.01.036

[38] T.N. Mtshali, I. Krupa, A.S. Luyt. The effect of cross-linking on the thermal properties of LDPE/wax blends. Thermochimica Acta 2001; 380:47-54.
DOI: 10.1016/S0040-6031(01)00636-0

[39] S.M. Gawish, H. Avci, A.M. Ramadan, S. Mosleh, R. Monticello, F. Breidt, R. Kotek. Properties of antibacterial polypropylene/nanometal composite fibers. Journal of Biomaterials Science 2012; 23:43-61.
DOI: 10.1163/092050610X541944

[40] Y. Shi, B. Sun, Z. Zhou, L.M. Wangatia, L. Chen, M. Zhu. Polypropylene nanocomposites based on synthetic organic-soluble Ag nanocrystals with prominent β-nucleating effect: Quiescent crystallization and melting behavior. Journal of Macromolecular Science, Part B: Physics 2012; 51:2505-2518.
DOI: 10.1080/00222348.2012.680374

[41] J.E. An, G.W. Jeon, Y.G. Jeong. Preparation and properties of polypropylene nanocomposites reinforced with exfoliated graphene. Fibers and Polymers 2012; 13:507-514.
DOI: 10.1007/s12221-012-0507-z

[42] X. Chen, S. Wei, A. Yadav, R. Patil, J. Zhu, R. Ximenes, L. Sun, Z. Guo. Poly(propylene)/carbon nanofiber nanocomposites: Ex situ solvent-assisted preparation and analysis of electrical and electronic properties. Macromolecular Materials and Engineering 2011; 296:434-443.
DOI: 10.1002/mame.201000341

[43] M.J. Mochane, A.S. Luyt. Preparation and properties of polystyrene encapsulated paraffin wax as possible phase change material in a polypropylene matrix. Thermochimica Acta 2012; 544:63-70.
DOI: 10.1016/j.tca.2012.06.017

[44] M.E. Mngomezulu, A.S. Luyt, I. Krupa. Structure and properties of phase-change materials based on high density polyethylene, hard Fischer Tropsch paraffin wax, and wood flour. Polymer Composites 2011; 32:1155-1163.
DOI: 10.1002/pc.21134

[45] M.E. Mngomezulu, A.S. Luyt, I. Krupa. Structure and properties of phase change materials based on HDPE, soft Fischer-Tropsch paraffin wax, and wood flour. Journal of Applied Polymer Science 2010; 118:1541-1551.
DOI:10.1002/app.32521

[46] J.A. Molefi, A.S. Luyt, I. Krupa, Investigation of thermally conducting phase change materials based on polyethylene/wax blends filled with copper particles. Journal of Applied Polymer Science 2010; 116:1766-1774.
DOI: 10.10022/app.31653

[47] Y. Cai, L. Song, Q. He, D. Yang, Y. Hu. Preparation, thermal and flammability properties of a novel form-stable phase change materials based on high density polyethylene/poly(ethylene-co-vinylacetate)/organophilicmontmorillonite nano-composites/paraffin compounds. Energy Conversion and Management 2008; 49:2055-2062.
DOI: 10.1016/j.enconman.2008.02.013

[48] Y. Cai, Y. Hu, L. Song, H. Lu, Z. Chen, W. Fan. Preparation and characterizations of HDPE–EVA alloy/OMT nanocomposites/paraffin compounds as a shape stabilized phase change thermal energy storage material. Thermochimica Acta 2006; 451:44-51.
DOI: 10.1016/j.tca.2006.08.015

[49] L. Zhang, J. Zhu, W. Zhou, J. Wang. Characterization of polymethyl methacrylate/polyethylene glycol/aluminum nitride composite as form-stable phase change material prepared by in situ polymerization. Thermochimica Acta 2011; 524:128-134.
DOI:10.1016/j.tca.2011.07.003

[50] L. Zhang, J. Zhu, W. Zhou, J. Wang, Y. Wang. Thermal and electrical conductivity enhancement of graphite nanoplatelets on form-stable polyethylene glycol/polymethyl methacrylate composite phase change materials. Energy 2012; 39:294-302.
DOI: 10.1016/j.energy.2012.01.011

[51] W. Mhike, W.W. Focke, J.P. Mofokeng, A.S. Luyt. Thermally conductive phase-change materials for energy storage based on low-density polyethylene, soft Fischer-Tropsch wax and graphite. Thermochimica Acta 2012; 527:75-82.
DOI: 10.1016/j.tca.2011.10.008

[52] K. Chrissafis, K.M. Paraskevopoulos, S.Y. Stavrev, A. Docoslis, A. Vassiliou, D.N. Bikiaris. Characterization and thermal degradation mechanism of isotactic polypropylene/carbon black nanocomposites. Thermochimica Acta 2007; 465:6-17.
DOI: 10.1016/j.tca.2007.08.007

[53] V. Vladimirov, C. Betchev, A. Vassiliou, G. Papageorgiou, D. Bikiaris. Dynamic mechanical and morphological studies of isotactic polypropylene/fumed silica nanocomposites with enhanced gas barrier properties. Composites Science and Technology 2006; 66:2935-2944.
DOI: 10.1016/j.compscitech.2006.02.010

[54] A. Vassiliou, D. Bikiaris, K. Chrissafis, K.M. Paraskevopoulos, S.Y. Stavrev, A. Docoslis. Nanocomposites of isotactic polypropylene with carbon nanoparticles exhibiting enhanced stiffness, thermal stability and gas barrier properties. Composites Science and Technology 2008; 68:933-943.
DOI: 10.1016/j.compscitech.2007.08.019

[55] Y. Liu, M. Kontopolou. The structure and physical properties of polypropylene and thermoplastic olefin nano-composites containing nanosilica. Polymer 2006; 47:7731-7739.
DOI: 10.1016/j.polymer.2006.09.014

[56] M. Jouni, A. Boudenne, G. Boiteux, V. Massardies, B. Garnier, A. Serghei. Electrical and thermal properties of polyethylene/silver nanoparticle composites. Polymer composites 2013; 34:778-786.
DOI:10.1002/pc.22478

[57] J.A. Molefi, A.S. Luyt, I. Krupa. Comparison of the influence of Cu micro- and nano-particles on the thermal properties of polyethylene/Cu composites. eXPRESS Polymer Letters 2009; 3:639-649
DOI: 10.3144/expresspolymlett.2009.80

[58] D. Bikiaris, A. Vassiliou, K. Chrissafis, K.M. Paraskevopoulos, A. Jannakoudakis, A. Docoslis. Effect of acid treated multi-walled carbon nanotubes on the mechanical, permeability, thermal properties and thermo-oxidative stability of isotactic polypropylene. Polymer Degradation and Stability 2008; 93:952-967.
DOI: 10.1016/j.polymdegradstab.2008.01.033

[59] D.W. Chae, B.C. Kim. Physical properties of isotactic poly(propylene)/silver nanocomposites: Dynamic crystallization behavior and resultant morphology. Macromolecular Materials and Engineering 2005; 290:1149-1156.
DOI: 10.1002/mame.200500277

[60] M.E. Achaby, F.E. Arrakhiz, S. Vaudreuil, A.K. Qaiss, M. Bousmina, O.F. Fehri. Mechanical, thermal, and rheological properties of graphene-based polypropylene nanocomposites. Polymer Composites 2012; 33:733-744.
DOI: 10.1002/pc.22198

[61] S.C. Tjong, S. Bao. Structure and mechanical behavior of isotactic polypropylene composites filled with silver nanoparticles. e-Polymers 2007; 7:1618-1634.
DOI: 10.1515/epoly.2007.7.1.1618

[62] J. Arranz-Andrés, B. Peña, R. Benavente, E. Pérez, M.L. Cerrada. Influence of isotacticity and molecular weight on the properties of metallocenic isotactic polypropylene. European Polymer Journal 2007; 43:2357-2370.
DOI: 10.1016/j.europolymj.2007.03.034

[63] A. Mollova, R. Androsch, D. Mileva, M. Gahleitner, S.S. Funari. Crystallization of isotactic polypropylene containing beta-phase nucleating agent at rapid cooling. European Polymer Journal 2013; 49:1057-1065.
DOI: 10.1016/j.eurpolymj.2013.01.015

[64] A. Saleem, L. Frormann, A. Iqbal. Mechanical, thermal and electrical resistivity properties of thermoplastic composites filled with carbon particles. Journal of Polymer Research 2007; 14:121-127.

DOI: 10.1007/s10965-006-9091-5

[65] M.A. Milani, D. González, R. Quijada, N.R.S. Basso, M.L. Cerrada, D.S. Azambuja, G.B. Galland. Polypropylene/graphene nanosheet nanocomposites by in situ polymerization: Synthesis, characterization and fundamental properties. Composites Science and Technology 2013; 84:1-7.
DOI: 10.1016/j.compscitech.2013.05.001

[66] A.S. Luyt, M.D. Dramićanin, Ž. Antić, V. Djoković. Morphology, mechanical and thermal properties of composites of polypropylene and nanostructured wollastonite filler. Polymer Testing 2009; 28:348-356.
DOI: 10.1016/j.polymertesting.2009.01.010

[67] L. Wang, J. Sheng. Preparation and properties of polypropylene/org-attapulgite nanocomposites. Polymer 2005; 46:6243-6249.
DOI: 10.1016/j.polymer.2005.05.067

[68] M. Du, B. Guo, X. Cai, X. Jia, M. Liu, D. Jia. Morphology and properties of halloysite nanotubes reinforced polypropylene nanocomposites. e-Polymers 2008; 1:1490-1503.
DOI: 10.1515/epoly.2008.8.8.1490

[69] D.W. Chae, S.S. Hwang, S.M. Hong, S.P. Hong, B.G. Cho, B.C. Kim. Influence of high contents of silver nanoparticles on the physical properties of poly(vinyl fluorine). Molecular Crystals and Liquid Crystals 2007; 464:233/[815]-241/[823].
DOI: 10.1080/5421400601031140

[70] V. Causin, C. Marega. A. Marigo, G. Ferrara, A. Ferraro. Morphological and structural characterization of polypropylene/conductive graphite nanocomposites. European Polymer Journal 2006; 42:3153-3161.
DOI: 10.1016/j.eurpolymj.2006.08.07

[71] P. Song, Z. Cao, Y. Cai, L. Zhao, Z. Fang, S. Fu. Fabrication of exfoliated graphene-based polypropylene nanocomposites with enhanced mechanical and thermal properties. Polymer 2011; 52:4001-4010.
DOI: 10.1016/j.polymer.2011.06.045

[72] C.H. Kang, K.H. Yoon, Y.B. Park, D.Y. Lee, S.S. Jeong. Properties of polypropylene composites containing aluminum/multiwalled carbon nanotubes. Composites Part A: Applied Science and Manufacturing 2010; 41:919-926.

DOI: 10.1016/j.compositesa.2010.03.011

[73] E. Logakis, E. Pollatos, Ch. Pandis, V. Peoglos, I. Zuburtikudis, C.G. Delides, A. Vatalis, M. Gjoka, E. Syskakis, K. Viras, P. Pissis. Structure-property relationships in isotactic polypropylene/multi-walled carbon nanotubes nanocomposites. Composites Science and Technology 2010; 70:328-335.
DOI: 10.1016/j.compscitech.2009.10.023

[74] M. Antunes, M. Mudarra, J.I. Velasco. Broad band electrical conductivity of carbon nanofibre reinforced polypropylene foams. Carbon 2011; 49:708-717.
DOI: 10.1016/j.carbon.2010.10.032

[75] S. Zhao, F. Chen, C. Zhao, Y. Huang, J.Y. Dong, C.C. Han. Interpenetrating network formation in isotactic polypropylene/graphene composites. Polymer 2013; 54:3680-3690.
DOI: 10.1016/j.polymer.2013.04.059

[76] D. Wang, X. Zhang, J.W. Zha, J. Zhao, Z.M. Dang, G.H. Hu. Dielectric properties of reduced graphene oxide/polypropylene composites with ultralow percolation threshold. Polymer 2013; 54:1916-1922.
DOI: 10.1016/j.polymer.2013.02.012

[77] E. Pollatos, E. Logakis, P. Chatzigeorgiou, V. Peoglos, I. Zuburtikudis, M. Gjoka, K. Viras, P. Pissis. Morphological, thermal, and electrical characterization of syndiotactic polypropylene/multiwalled carbon nanotube composites. Journal of Macromolecular Science, Part B: Physics 2010; 49:1044-1056.
DOI: 10.1080/00222341003609708

[78] C.R. Yu, D.M. Wu, Y. Liu, H. Qiao, Z.Z. Yu, A. Dasari. X.S. Du, Y.W. Mai. Electrical and dielectric properties of polypropylene nanocomposites based on carbon nanotubes and barium titanate nanoparticles. Composites Science and Technology 2011; 71:1706-1712.
DOI: 10.1016/j.compscitech.2011.07.022

[79] V.G. Shevchenko, S.V. Polschikov, P.M. Nedorezova, A.N. Klyamkina, A.N. Shchegolikhin, A.M. Aladyshev, V.E. Muradyan. In situ polymerized poly(propylene)/graphene nanoplatelets nanocomposites: Dielectric and microwave properties. Polymer 2012; 53:5330-5335.
DOI: 10.1016/j.polymer.2012.09.018

CHAPTER 2

Materials and methods

2.1 Materials

Isotactic polypropylene with a melt flow index of 12g/10 min (230 °C/2.16 kg), density of 0.9 g cm^{-3} and melting point of ~160 °C was supplied by Sasol polymers.

Medium-soft paraffin wax (M3 wax) was supplied in powder form by Sasol Wax. It consists of approximately 99% of straight chain hydrocarbons and few branched chains. It has an average molar mass of 440 g mol^{-1} and a carbon distribution between C15 and C78. Its density is 0.90 g cm^{-3} and it has a melting point range around 40-60 ºC.

The 99.99 % pure silver (Ag) nanoparticles with particle size 30-50 nm was supplied by Dong Yang (HK) Int'l group limited in China.

2.2 Composite preparation

All the samples were prepared by melt mixing using a Brabender Plastograph with 55 ml internal mixer. The samples were mixed for 15 min. in the proportions represented in Table 2.1 at 190 °C and a mixing speed of 50 rpm. The Ag powder was exposed to ultra-sonication for 6 hours prior to the sample preparation. For the blends, the components were premixed and then fed into the heated mixer, whereas for the composites, the Ag nanoparticles were added into the Brabender mixer 10 minutes after adding the premixed iPP/wax blends. The samples were then melt pressed at 190 °C for 5 minutes under 50 kPa using a hydraulic melt press. The prepared samples were then exposed to two thermal treatments, either quenching in ice water or slow cooling from the melt at 190 to 100 °C.

Table 2.1 Sample ratios used for the preparation of the blends and composites

iPP (w/w)	**iPP/wax (w/w)**
100	95/5
	90/10
	80/20
iPP/Ag (w/w)	**iPP/wax/Ag (w/w)**
98/2	88/10/2
97/3	87/10/3
96/4	86/10/4
95/5	85/10/5

2.3 Characterization techniques

2.3.1 Transmission electron microscopy (TEM)

TEM is a high resolution electron microscopy technique which forms an image through an electron beam that passes through the sample [1]. In TEM experiments, the electrons are emitted by an electron gun, commonly fitted with a tungsten filament cathode as the electron source. In order to allow proper image formation, the sample thickness is limited to a few hundred nanometers [2]. TEM provides atomic scale resolution, combined with nano-scale crystal structure elucidation through convergent beam electron diffraction (CBED), chemical information through energy dispersive spectroscopy (EDS), and electronic structure elucidation through electron energy loss spectroscopy (EELS). It involves two techniques, planar view and cross-section TEM. Planar view TEM provides a relatively large view area of a thin film normal to its surface and gives information about the grain size and distribution of defects. Cross-section TEM is a technique which is used to study film thickness, step coverage, implant damage, and etch profiles via contact filing, interface contamination, particle identification and failure analysis [3].

For the TEM analysis the samples were sectioned at 150 nm using a Leica UC7 (Viennna, Australia) ultramicrotome, and examined with a Philips (FEI) (Eindhoven, The Netherlands) CM 100 transmission electron microscope at 60 keV.

2.3.2 Differential scanning calorimetry (DSC)

DSC is an analytical technique which gives information about the heat capacity, glass transition, melting, crystallization, enthalpy and entropy changes in materials [4]. A DSC technique provides a curve showing endothermic and exothermic peaks, and baseline shifts due to the occurrence of chemical and physical reactions in various steps [5]. There are two types of the commonly used DSCs, i.e. power compensation and heat flux. A power compensation DSC consists of the two separate identical holders i.e. the sample and reference holders, each with its own heater and sensor. A heat flux DSC is composed of sample and reference holders separated by a bridge that acts as a heat leak surrounded by a block that is a constant-temperature body [6]. In a DSC the experiments are carried out using aluminium, copper or steel pans in various inert or oxidizing atmospheres [7-9].

The DSC analyses of all the blends and composites were done using a Perkin-Elmer DSC 7 differential scanning calorimeter. The experiments were done under a nitrogen atmosphere with a flow rate of 20 ml min^{-1}. The instrument was computer controlled and all the calculations were done using Pyris software. Samples with masses of 5-10 mg were sealed in aluminium pans. All the samples were heated from 20 to 180 °C at a heating rate of 20 °C min^{-1}, and cooled at 30 °C min^{-1}. The peak temperatures of melting and crystallization, as well as the enthalpies of melting and crystallization, were determined from the first heating scan. All the measurements were repeated three times for each sample. The melting and crystallization temperatures, as well as enthalpies, are reported as average values with standard deviations.

2.3.3 Dynamic mechanical analysis (DMA)

DMA is an analytical technique used to determine the low-strain thermomechanical properties of materials as a function of frequency, temperature or time [10-12]. The thermomechanical

properties are determined by either applying a small oscillating strain to the sample and measuring the resulting stress, or a periodic stress and measuring the resulting strain [11-13]. The dynamic complex modulus measured by DMA instrument is divided into the storage modulus (E'),which corresponds to the elastic modulus which is proportional to the energy fully recovered per cycle, and loss modulus (E"), which is proportional to the net energy dissipated per cycle in the form of heat. The loss tangent is given by tan $\delta = E''/E'$. The occurrence of molecular mobility transitions such as the glass transition temperature (T_g) is usually determined from the loss modulus and tangent curves [14,15].

The dynamic mechanical properties of the blends and composites were investigated using a Perkin Elmer Diamond DMA. The analyses were performed from -40 to 140 °C in bending (dual cantilever) mode at a heating rate of 3 °C min^{-1} and a frequency of 1 Hz.

2.3.4 Thermal conductivity

Thermal conductivity is a measure of thermal heat transport property of a material. There are two techniques that are usually used to measure the thermal conductivity i.e. the steady-state and transient methods. The steady state method involves the radial heat flow and heat guarded hot plate methods. The hot disk technique, which is a transient plane source, uses a metal strip or disk as a continuous plane heat source as well as a temperature monitor [16,17]. The temperature change can be accurately measured by determining the electric resistance across the hot disk sensor. The information on the thermal heat transport properties of the material surrounding the hot disk sensor can be determined by monitoring the temperature increase over a short period of time after the start of the experiment. The hot disk technique gives accurate measurements, has shorter test times, and can measure thermal conductivities of small samples. It has been successfully used to measure the thermal conductivities of various materials with low electrical conductivity (such as fused quartz), building materials (e.g. cement and brick powder), stainless steel, copper powder, anisotropic solids (crystalline quartz), and thin metallic materials [16-18].

The thermal conductivity measurements were done using a Therm Test Inc. Hot Disk TPS 500 thermal constant analyzer. The hot disk sensor used in this study was a Kapton sensor with a

radius of 3.2 mm and the samples with 10 mm thickness and a diameter of 13 mm were used for the analysis. The sensor was placed between two samples of the same composition. The measurements were done for 20 s in order to prevent the heat flow from reaching the boundary of the samples. All the measurements were repeated ten times for each sample. The thermal conductivities are reported as average values with standard deviations.

2.3.5 Dielectric properties

Dielectric properties refer to the variation of direct current (DC), alternating current (AC) and electric breakdown strength as a function of frequency, composition, voltage, pressure and temperature [1]. They give information about the orientation and translational adjustment of the mobile charge present in the dielectric medium [19]. Dielectric properties are usually measured using impedance spectroscopy, which is a very powerful technique in solid state electronic systems. It correlates the dielectric properties of a material with its microstructure, and analyzes the separate the contributions from various components i.e. through grains, grain boundaries and interfaces over a wide frequency range [20,21].

Samples in the form of discs (D = 13 mm, d = 1 mm) were cut from the centre of the melt-pressed sheets. The surfaces of the samples were made conductive using soft graphite. Dielectric measurements were done using an Agilent 4263B dielectric spectroscopy instrument in the frequency range between 1 kHz and 17 MHz at room temperature, and with an applied voltage of 1 V. Conductance (G) and susceptance (B) were measured and the AC conductivity (σ_{ac}) was calculated as $\sigma_{ac}= \sqrt{B^2 + G^2}$ and the following relations were derived: $\tan\delta = G/B$ and $B = 2\pi fC$, where f is the frequency and C is the capacitance, and $C = \varepsilon'\varepsilon_o S/d$, where ε' is the real part of the dielectric permittivity, ε_o the vacuum permittivity and S/d describing the geometry of the samples ($S = \pi D^2/4$). DC measurements were done using a Keithley 2401 amperemeter during 10 s of electric field application at 200 V mm^{-1}.

2.4 References

[1] C.E. Carraher, Jr. Carraher's Polymer Chemistry. CRC Press, New York (2011).

[2] V. Klang, C. Valenta, N.B. Matsko. Electron microscopy of pharmaceutical systems. Micron 2013; 44:45-74.
DOI: 10.1016/j.micron.2012.07.008

[3] H. Zhang. What limits the application of TEM in the semiconductor industry? Thin Solids Films 1998; 320:77-85.
DOI: 10.1016/S0040-6090(97)01073-0

[4] C. Schick. Differential scanning calorimetry (DSC) of semicrystalline polymers. Analytical and Bioanalytical Chemistry 2009; 395:1589-1611.
DOI: 10.1007/s00216-009-3169-y

[5] T. Arii, A. Kishi, Y. Kobayashi. A new simultaneous apparatus for X-ray diffractometry and differential scanning calorimetry (XRD-DSC). Thermochimica Acta 1999; 325:151-156.
DOI: 10.1016/S0040-6031(98)00573-5

[6] J.D. Menczel, R.B. Prime. Thermal Analysis of Polymers. Fundamentals and Applications. John Wiley & Sons, New Jersey (2009).

[7] R.J. Young, P.A. Lovell. Introduction to Polymers. CRC Press, New York (2011).

[8] R.L. Danley. New heat flow DSC measurement technique. Thermochimica Acta 2003; 395:201-208.
DOI: 10.1016/S0040-6031(02)00212-5

[9] S.D. Pandita, L. Wang, R.S. Mahendran, V.R. Machavaram, M.S. Irfan, D. Harris, G.F. Fernando. Simultaneous DSC-FTIR spectroscopy: Comparison of cross-linking kinetics of an epoxy/amine resin system. Thermochimica Acta 2012; 543:9-17.
DOI: 10.1016/j.tca.2012.04.024

[10] N. Soutari, A.B.M. Buanz, M.O. Gul, C. Tuleu, S. Gaisford. Quantifying crystallisation rates of amorphous pharmaceuticals with dynamic mechanical analysis. International Journal of Pharmaceutics 2012; 423:335-340.
DOI:10.1016/j.ijpharm.2011.11.010

[11] P. Lee-Sullivan, D. Dykeman. Guidelines for performing storage modulus measurements using the TA Instruments DMA 2980 three-point bend mode I. Amplitude effects. Polymer Testing 2000; 19:155-164.
DOI: 10.1016/S0142-9418(98)00083-X

[12] S. Deng, M. Hou, L. Ye. Temperature-dependent elastic moduli of epoxies measured by DMA and their correlations to mechanical testing data. Polymer Testing 2007; 26:803-813.
DOI: 10.1016/j.polymertesting.2007.05.003

[13] R.L. Sakaguchi, N.C. Shah, B.S. Lim, J.L. Ferracane, S.E. Borgersen. Dynamic mechanical analysis of storage modulus development in light-activated polymer matrix composites. Dental Materials 2002; 18:197-202.
DOI: 10.1016/S0109-5641(01)00082-3

[14] A.B. Bashoiwddu, F. Podczeck. J.M. Newton. Application of dynamic mechanical analysis (DMA) to determine the mechanical properties of pellets. Journal of Pharmaceutics 2004; 269:329-342.
DOI:10.1016/j.ijpharm.2003.09.028

[15] P.S. Thomas, S. Thomas, S. Bandyopadhya, A. Wurm, C. Schick. Polystyrene/calcium phosphate nanocomposites: Dynamic mechanical and differential scanning calorimetric studies. Composites Science and Technology 2008; 68:3220-3229.
DOI: 10.1016/j.compscitech.2008.08.008

[16] Y. He. Rapid thermal conductivity measurement with a hot disk sensor Part 1. Theoretical considerations. Thermochimica Acta 2005; 436:122-129.
DOI: 10.1016/j.tca.2005.06.026

[17] M. Rides, J. Morikawa, L. Halldahl, B. Hay, H. Lobo, A. Dawson, C. Allen. Intercomparison of thermal conductivity and thermal diffusivity methods for plastics. Polymer Testing 2009; 28:480-489.
DOI: 10.1016/j.polymertesting.2009.03.002

[18] Y. He. Rapid thermal conductivity measurement with a hot disk sensor Part 2. Characterization of thermal greases. Thermochimica Acta 2005; 436:130-134.
DOI: 10.1016/j.tca.2005.06.026.

[19] A.A.A. Darwish, E.F.M. El-Zaidia, M.M. El-Nahass, T.A. Hanafy, A.A. Al-Zubaidi. Dielectric and electrical conductivity studies of bulk lead (II) oxide (PbO). Journal of Alloys and Compounds 2014; 589:393-398.
DOI: 10.1016/j.jallcom.2013.11.218

[20] M.M. El-Nahass, H.S. Metwally, H.E.A. El-Sayed, A.M. Hassanien. Electrical conductivity and dielectric relaxation of bulk iron(III)chloride tetraphenylporphyrin. Materials Chemistry and Physics 2012; 133:649-654.
DOI: 10.1016/j.matchemphys.2012.01.042

[21] K.C. Verma, M.T. Ram, J. Singh, R.K. Kotnala. Impedance spectroscopy and dielectric properties of Ce and La substituted $Pb_{0.7}Sr_{0.3}(Fe_{0.012}Ti_{0.988})O_3$ nanoparticles. Journal of Alloys and Compounds 2011; 509:4967-4971.
DOI: 10.1016/j.jallcom.2011.01.144

CHAPTER 3

Results and discussion

3.1 Transmission electron microscopy (TEM)

Figure 3.1 shows the TEM images of some of the investigated nanocomposites that were slowly cooled from the melt. The TEM image of the iPP/Ag nanocomposite containing 2 wt% nanoparticles shows iPP spherulites containing Ag nanoparticles at their growth centres (Figure 3.1a, arrow A). It looks as if primary nucleation could have started at the nanoparticles that formed nucleation centres from which the spherulitic growth evolved [1]. Ag nanoparticles (with diameters ranging from 0.09 to 1.15μm) can also be seen on the edges of the iPP spherulites, but they are fairly well dispersed, although some obvious aggregates are visible. However, at a higher Ag content (Figure 3.1b) there are fewer individual Ag particles and more of the filler aggregates (with diameters ranging from 0.12 to 3.11 μm). The nanoparticles have a tendency of forming aggregates because they have a higher affinity for each other than for the matrix.

In the iPP/wax nanocomposites (Figure 3.1c) the wax probably crystallized separately in the areas between the iPP spherulites. This separate crystallization of the wax can be expected because iPP crystallizes before the wax. The presence of a molten wax during the crystallization must have influenced the crystal growth of the iPP by acting as a plasticizer, and therefore the spherulites in Figure 3.1c seem to be smaller and somewhat differently structured from the spherulites in Figure 3.1a. Individual Ag nanoparticles and some aggregates (with diameters ranging from 0.11 to 1.53 μm) are observed in Figure 3.1c. These nanoparticles are only dispersed in between the spherulites (arrow B), with none visible at the growth centres of the spherulites. The nanoparticles seem to have a higher affinity for the wax, and therefore remained in the molten wax phase during the crystallization of iPP. They were then trapped in the wax phase after wax crystallization. However, at higher Ag content the filler particles (with diameters ranging from 0.11 to 1.72 μm) were not well dispersed and the extent of agglomeration increased (Figure 3.1d). Nanoparticles are also visible at the growth centres of the PP spherulites (arrow C).

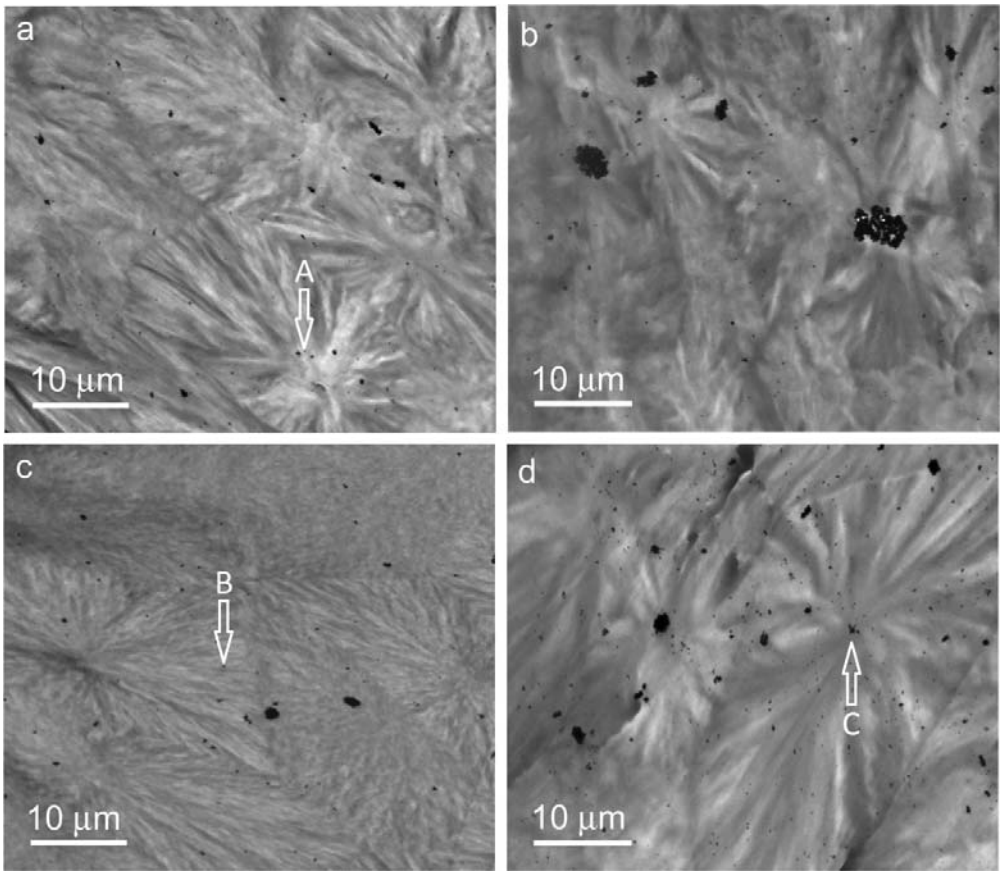

Figure 3.1 TEM images of (a) 98/2 w/w iPP/Ag, (b) 95/5 w/w iPP/Ag, (c) 88/10/2 w/w iPP/Wax/Ag, and (d) 85/10/5 w/w iPP/Wax/Ag slowly cooled from the melt

3.2 Differential scanning calorimetry (DSC)

The DSC heating curves of the iPP/wax blends that were quenched and slowly cooled from the melt are shown in Figure 3.2. The iPP/wax blends with 5 wt% wax show a single melting peak which is associated with the melting of the iPP crystals. This indicates that the wax and iPP are probably miscible in the molten state. However, when the wax content is 10 wt% and more, two separate melting peaks appear at lower and higher temperatures. These are associated with the melting of wax and iPP crystals, respectively. This is observed in both the slowly cooled and quenched samples. The observed behaviour indicates the (partial) immiscibility of the blend components. From this it is clear that iPP and wax are probably miscible up to 5 wt% wax. At higher wax contents there is a partial immiscibility and most of the wax crystallized separately from iPP. Moreover, the melting peaks corresponding to the melting of iPP crystals shifted to

lower temperatures with an increase in wax content. This is attributed to the plasticization effect of the paraffin wax [2-4].

At lower wax contents, the normalised melting enthalpies of the wax component are lower than that of pure wax (Table 3.1). However, at 20% wax content, they are comparable to that of pure wax. This is probably because the individual wax chains are trapped in the amorphous phase of iPP, or co-crystallized with iPP chains, at low wax content and as a result only a small portion of the wax crystallized separately. However, at a higher content, more wax crystallized separately from iPP. The normalized melting enthalpies of the iPP component increased with an increase in wax content (Table 3.1). This confirms the co-crystallization of some of the wax with iPP giving rise to the higher melting enthalpy of iPP. The normalised melting enthalpies of the iPP component in the slowly cooled blends are higher than the comparable blends quenched from the melt. This is attributed to the higher crystallinity of the blends slowly cooled from the melt. In the slow cooling process there is enough time for the crystals to form, whereas faster cooling such as quenching reduces the time for crystal nucleation and growth [5,6].

The iPP/wax/Ag nanocomposites containing 10 wt% wax, that were quenched and slowly cooled from the melt, are shown in Figure 3.3. Both the slowly cooled and quenched samples show two separate melting peaks associated with the melting of wax and iPP crystals. There are no significant changes in the melting temperatures and normalised enthalpies of the iPP component with an increase in Ag content for both the quenched and slowly cooled samples (Table 3.1). This indicates that the presence of Ag nanoparticles had little influence on the crystallite sizes and mobility of the polymer chains. However, if the normalized enthalpies of the quenched and slowly cooled samples are compared, it is clear that the melting enthalpies of the slowly cooled samples are higher those of the quenched samples. This is the result of the higher crystallinity of the slowly cooled samples. The crystallization and melting temperatures of the quenched and slowly cooled iPP/wax blends and iPP/wax/Ag blend composites are very similar within experimental error, although the values are slightly lower at higher wax content for the iPP/wax blends (Table 3.1). Wax normally acts as a plasticizer by enhancing the mobility of the polymer chains, leading to lower crystallization and melting temperatures. However, when Ag nanoparticles are present, they can act as the nucleating sites for the crystallization of iPP, and

this will give rise to higher crystallization and melting temperatures. It therefore seems as if the opposing effects of wax and Ag on iPP crystallization balance each other in the iPP/wax/Ag blend composites, which causes the crystallization and melting temperatures of iPP to remain unchanged.

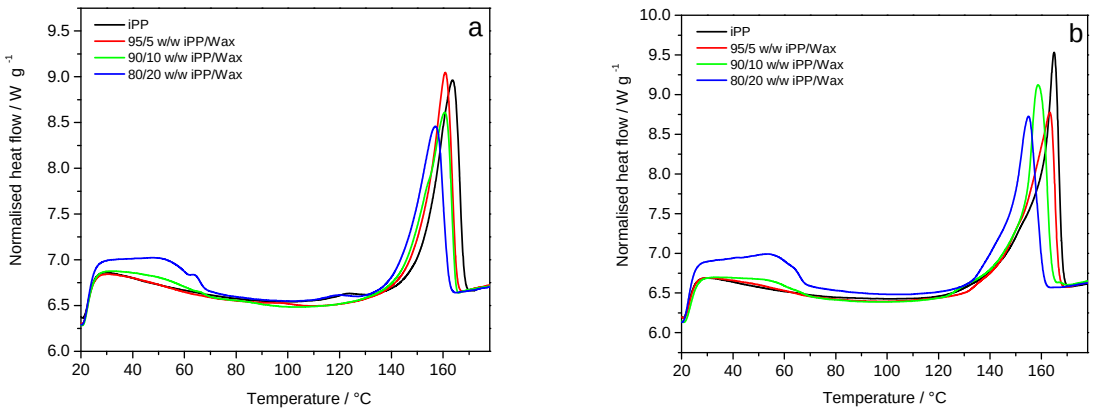

Figure 3.2 Heating curves of iPP and iPP/wax blends (a) quenched and (b) slowly cooled from the melt

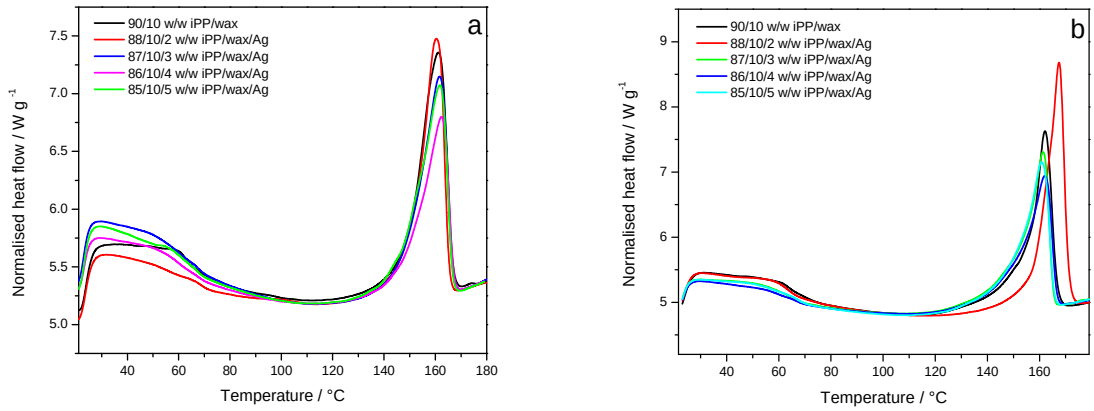

Figure 3.3 Heating curves of iPP and 10 wt% wax containing iPP/Ag nanocomposites (a) quenched and (b) slowly cooled from the melt

Table 3.1 DSC melting and crystallization parameters of the investigated samples

Sample w/w	T_m / °C		ΔH_m / J g^{-1}		ΔH^n_m / J g^{-1}		T_c / °C	
	Quenched	**Slowly cooled**	**Quenched**	**Slowly cooled**	**Quenched**	**Slowly cooled**	**Quenched**	**Slowly cooled**
iPP	163.7 ± 0.6	163.9 ± 1.1	79.3 ± 6.7	100.0 ± 5.1	-	-	104.6 ± 0.8	102.1 ± 1.2
Wax	60.7 ± 0.4	60.7 ± 0.4	137.5± 7.6	137.5± 7.6	-	-	43.2 ± 0.8	43.2 ± 0.8
iPP/wax								
95/5	161.0 ± 0.6	160.8 ± 0.2	81.3 ± 3.5	96.9 ± 2.2	85.6	102.0	107.2 ± 0.3	99.7 ± 0.6
90/10	59.3[a] ± 0.8 161.1[b] ± 0.4	55.0[a] ± 0.3 161.0[b] ± 1.0	5.9 ± 3.6 83.5 ± 3.7	6.9 ± 0.7 86.0 ± 3.0	59.0 92.8	69.0 95.6	43.7[a] ± 0.3 103.2[b] ± 0.3	42.2[a] ± 0.3 102.2[b] ± 4.9
80/20	56.6[a] ± 3.2 158.2[b] ± 0.8	59.7[a] ± 3.2 157.3[b] ± 1.9	12.0 ± 1.8 82.2 ± 3.2	17.6 ± 6.1 100.2 ±5.3	120.0 102.8	176.0 125.3	41.6[a] ± 0.3 99.4[b] ± 3.5	40.9[a] ± 0.5 97.2[b] ± 0.8
iPP/wax/Ag								
88/10/2	51.0[a] ± 0.4 160.2[b] ± 0.2	55.3[a] ± 0.3 166.2[b] ± 1.4	1.7 ± 0.2 74.1 ± 3.1	6.0 ± 0.2 92.8 ± 1.7	17.0 84.2	60.0 105.5	45.2[a] ± 0.6 105.6[b] ± 0.3	42.6[a] ± 0.3 100.1[b] ± 0.3
87/10/3	51.6[a] ± 0.2 161.9[b] ± 0.2	53.7[a] ± 0.9 162.1[b] ± 0.7	4.3 ± 0.3 71.7 ± 1.0	4.4 ± 0.9 83.8 ± 4.3	43.0 82.4	44.0 96.3	43.1[a] ± 0.3 98.9[b] ± 0.5	43.4[a] ± 0.5 100.4[b] ± 1.1
86/10/4	54.9[a] ± 2.8 162.5[b] ± 0.9	54.0[a] ± 1.2 162.1[b] ± 0.7	3.4 ± 1.3 72.5 ± 8.0	5.4 ± 2.0 82.5 ± 3.4	34.0 84.3	54.0 95.9	43.1[a] ± 0.3 100.9[b] ± 0.9	42.2[a] ± 0.3 100.1[b] ± 0.3
85/10/5	54.8[a] ± 1.6 162.0[b] ± 0.1	53.1[a] ± 0.7 160.5[b] ± 0.7	3.8 ± 0.5 69.4 ± 1.3	4.4 ± 1.0 83.4 ± 3.9	38.0 81.6	44.0 98.1	44.1[a] ± 0.3 101.9[b] ± 0.5	44.2[a] ± 0.3 101.9[b] ± 0.5
iPP/Ag								
98/2	165.0 ± 0.5	165.3 ± 0.7	79.6 ± 1.6	97.2 ± 2.9	81.2	99.2	106.7 ± 0.8	104.2 ± 0.3
97/3	165.3 ± 0.4	165.3 ± 0.7	73.7 ± 5.8	95.0 ± 3.0	76.0	97.9	107.7 ± 0.3	106.7 ± 0.6
96/4	167.3 ± 1.9	165.8 ± 1.2	75.1 ± 2.0	95.0 ± 3.2	78.2	99.0	107.9 ± 0.9	108.1 ± 0.3
95/5	165.6 ± 0.7	167.1 ± 1.4	73.3 ± 2.6	89.9 ± 2.7	77.2	94.6	107.4 ± 0.5	106.6 ± 0.3

T_m-melting peak temperature, T_c-crystallization peak temperature, ΔH^n_m-melting enthalpy normalised with respect to PP content

[a] Melting/crystallization of wax.

[b] Melting/crystallization of PP

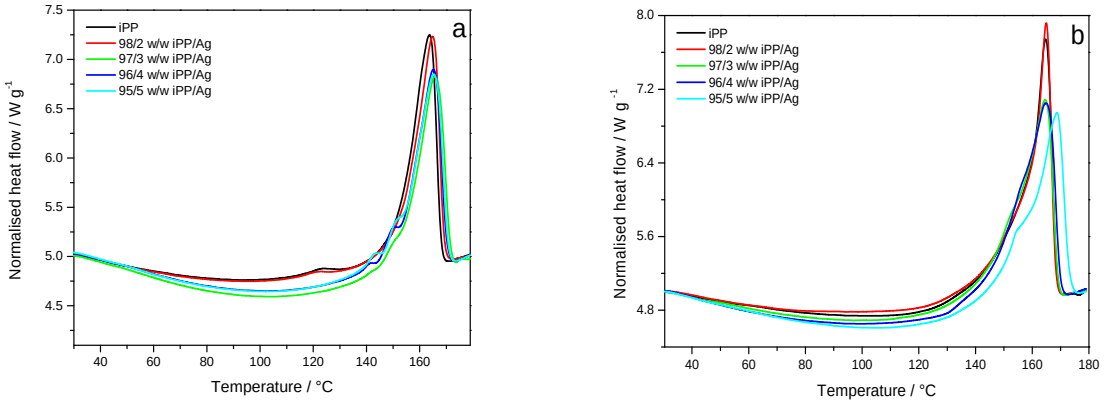

Figure 3.4 Heating curves of iPP and the iPP/Ag nanocomposites (a) quenched and (b) slowly cooled from the melt

The DSC heating curves of the iPP/Ag nanocomposites, that were quenched and slowly cooled from the melt, are shown in Figure 3.4. Both the quenched and slowly cooled iPP/Ag nanocomposites show a single melting peak associated with the melting of the PP crystals. There are no significant differences between the enthalpies of iPP in the iPP/Ag nanocomposites and that of pure iPP for both the quenched and slowly cooled samples (Table 3.1). However, the melting and crystallization temperatures are slightly higher than that of pure iPP. It is clear from this observation that the presence of Ag nanoparticles reduces the iPP chain mobility, as already mentioned before. The melting enthalpies of the slowly cooled composites are higher than those of the comparable composites quenched from the melt. The reason for this has already been discussed.

3.3 Dynamic mechanical analysis (DMA)

The storage modulus of the quenched iPP shown in Figure 3.5a increases with the addition of 10 wt% wax. This is attributed to the increase in crystallinity because of the much higher crystallinity of the wax. However, the storage modulus of the iPP/Ag nanocomposites changed very little compared to that of pure iPP, which indicates that the nanoparticle content was too small and the interaction with the polymer was too weak to significantly influence the polymer stiffness. When both wax and Ag are present, the storage modulus of the nanocomposites is very

similar to that of the iPP/wax sample. This confirms that the highly crystalline wax provided more stiffness to the sample, while the small amount of Ag had very little influence.

In the slowly cooled samples, the storage modulus of the iPP/wax samples is significantly lower than that of iPP (Figure 3.5b). This could be attributed to a decrease in iPP crystallinity, or to a softening effect of the much softer wax. If one looks at the values in Table 3.1, it is clear that the normalised melting enthalpy of iPP in the 90/10 w/w iPP/wax sample is slightly lower than that of pure iPP, although very similar within experimental error. It is, therefore, doubtful that the decrease in storage modulus is the result of lower iPP crystallinity.

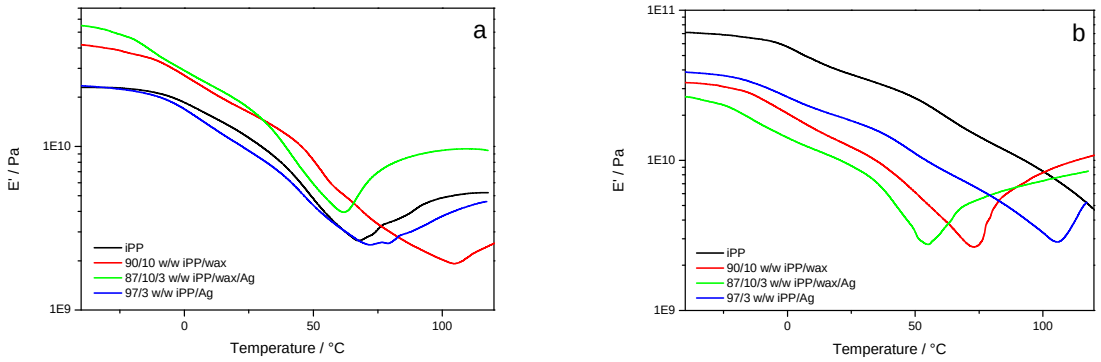

Figure 3.5 Storage modulus as a function of temperature of iPP, iPP/wax, iPP/Ag and iPP/wax/Ag samples (a) quenched and (b) slowly cooled from the melt

When comparing the storage modulus of the iPP/Ag sample with that of iPP and iPP/wax, it can be seen that it is lower than that of iPP, but higher than that of iPP/wax. According to Table 3.1 the melting enthalpies of iPP and iPP in iPP/wax and iPP/Ag are very similar, so differences in their storage moduli cannot be the result of differences in iPP crystallinity. It has been reported previously that the nanoparticles can have a plasticizing effect on a polymer [8], and therefore the lower storage modulus in the case of iPP/Ag is probably the result of such a plasticizing effect. However, this plasticizing effect is not as pronounced as the softening effect of the wax, therefore the storage modulus of iPP/Ag is still higher than that of iPP/wax. The storage modulus is the lowest when both wax and Ag are present. Again the melting enthalpy of iPP in iPP/wax/Ag is not much different from that of pure iPP (Table 3.1), and therefore the reduction in storage modulus cannot be the result of a change in crystallinity. It is expected that there will

be a very weak interaction between iPP and wax, while it seems as if there is a strong interaction between wax and Ag (section 3.1). The wax-covered Ag particles will then increase the free volume in the sample, which will give rise to higher iPP chain mobility in the amorphous phase and reduced stiffness.

The tan δ curves in Figure 3.6a show that the quenched iPP has two relaxation peaks associated with the β- and α-relaxations, respectively at about 10 and 70 °C. The β-relaxation is usually associated with motions within the amorphous regions during the glass transition, and the α-relaxation is related to the crystalline phase of the polymer [9,10]. When wax is present, an additional peak appeared at about 60 °C, which is associated with the wax melting. The β-peak of the iPP/wax sample looks very similar to that of pure iPP, and appears at about the same temperature, while the α-peak moved to higher temperatures. This indicates that the highly crystalline wax did not influence the iPP chain mobility in the amorphous phase, but in some way influenced the crystalline phase of iPP. According to Table 3.1 the normalised melting enthalpy of iPP in the blend is higher than that of the pure iPP, which could explain the increase in the α-transition temperature. The iPP/Ag sample also shows two relaxation peaks associated with the β- and α-relaxations. The temperature of the β-peak is very similar to that of iPP, but the α-peak appeared at a slightly higher temperature. This can be attributed to the dispersion of the Ag particles in the inter-crystalline amorphous areas of the iPP (as discussed in section 3.1), and therefore they will have an immobilizing effect on these chain segments. However, in the presence of both Ag and wax, only the β-relaxation and the wax melting peaks are visible. The α-peak is not visible in the investigated temperature range. The β-peak appeared at an observably lower temperature and the wax melting is much more prominent than that of the iPP/wax blend. It is expected that there will be a weak interaction between iPP and wax, while there is a stronger interaction between wax and Ag (see section 3.1). The wax-covered Ag particles will then increase the free volume in the sample, which will give rise to higher iPP chain mobility in the amorphous phase, leading to lower T_g values. It is not clear why the α-peak has disappeared, unless it has moved to an even higher temperature outside our analysis range.

The slowly cooled iPP has two relaxation peaks associated with the β- and α-relaxations at about 10 and 130 °C (Figure 3.6b). When wax is present there are also two relaxation peaks,

respectively associated with the glass transition and wax melting. The α-peak is not visible in the investigated temperature range, probably because wax has crystallized in the inter-crystalline amorphous regions of iPP, and as a result reduced the mobility on these chain segments. The β-peak of the iPP/wax sample is at a lower temperature than that of the pure iPP, which can be attributed to the increase in free volume because of the relatively weak interaction between iPP and wax, which gives rise to higher iPP chain mobility in the amorphous phase. The iPP/Ag nanocomposites also have two relaxation peaks associated with the β- and α-transitions. In this case both the β- and α-peaks appear at lower temperatures than those of pure iPP. This is an indication that Ag particles to some extent have plasticized iPP, giving rise to an increase in iPP chain mobility in the amorphous phase [8,11]. The decrease in the α-transition temperature must be related to the presence of the Ag particles in the inter-crystalline amorphous areas of iPP. It is, however, not clear exactly how these particles influenced the relaxation of the chains in these areas, since for the quenched samples the temperature of this transition increased. When both wax and Ag were present, the observation is similar to that of the quenched sample, and the explanation will be the same.

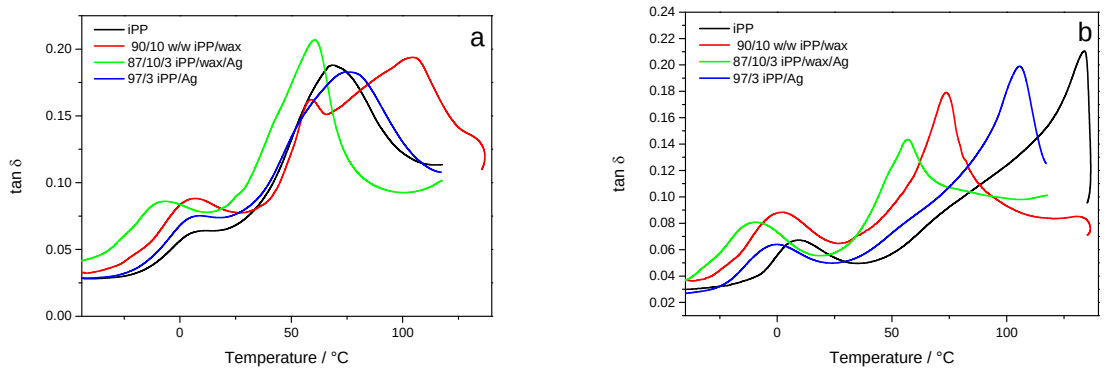

Figure 3.6 Loss factor as a function of temperature of iPP, iPP/wax, iPP/Ag and iPP/wax/Ag nanocomposites (a) quenched and (b) slowly cooled from the melt

Figure 3.7 compares the storage modulus curves of the quenched and slowly cooled samples. The storage modulus of the slowly cooled iPP and iPP/Ag nanocomposites is much higher than that of the quenched samples (Figures 3.7a and 3.7b). This is attributed to the higher crystallinity of the slowly cooled samples, as can be seen from the higher normalised melting enthalpies of the slowly cooled samples (Table 3.1). However, the quenched and slowly cooled iPP/wax

samples show almost the same modulus (Figure 3.7c), indicating that the presence of the soft wax counter-acted the influence of the higher crystallinity of the slowly cooled blend. When both wax and Ag are present, the storage modulus of the slowly cooled sample is significantly lower than that of the quenched sample (Figure 3.7d). According to Table 3.1 the normalised melting enthalpy of iPP in the slowly cooled iPP/wax/Ag is higher than that in the quenched sample, and the differences in storage modulus is therefore not related to the differences in crystallinity. The only possible reason for this observation is that more wax crystallized around the nanoparticles in the quenched samples, giving rise to more rigidity from the wax-covered Ag filler.

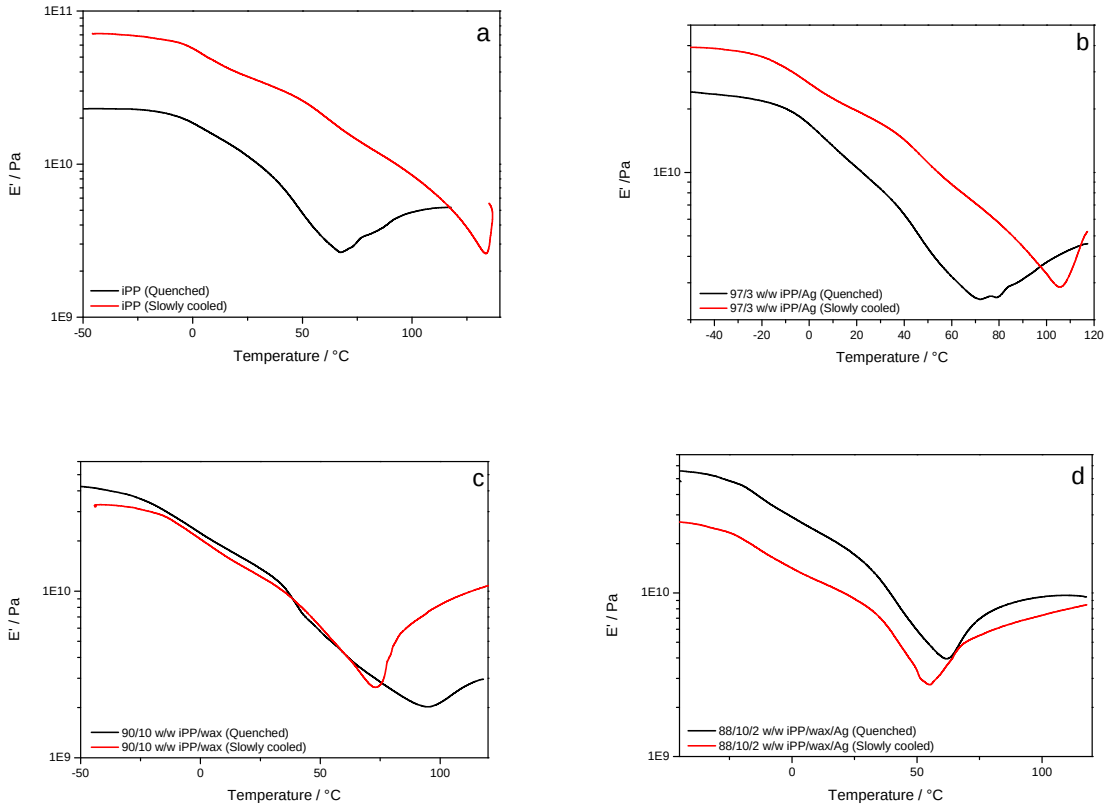

Figure 3.7 Storage modulus as a function of temperature of the quenched and slowly cooled (a) iPP, (b) iPP/wax, (c) iPP/Ag and (d) iPP/wax/Ag nanocomposites

There is no difference between the temperatures of the β-peaks in the quenched and slowly cooled iPP (Figure 3.8a), which is to be expected because differences in cooling rate will only influence the crystallinity of iPP. The α-peak of the slowly cooled iPP appears at a significantly higher temperature than that of the quenched iPP. This is attributed to the higher crystallinity of

the slowly cooled samples (compare melting enthalpy values in Table 3.1). If one compares the relaxation peaks of the iPP/Ag samples, it can be seen that the β-peak of the slowly cooled iPP/Ag sample appears at a lower temperature, but the α-peak is still at a higher temperature, than those of the quenched samples (Figure 3.8b). The difference between the α-peaks of the samples is attributed to the difference in crystallinity between the quenched and slowly cooled samples (Table 3.1), although Ag had an influence in both cases, as discussed before. Therefore, the presence of Ag particles in the inter-crystalline amorphous regions (section 3.1) influences the crystalline phase more than the amorphous phase in the slowly cooled sample, because of its higher crystallinity, but the amorphous phase more than the crystalline in the quenched sample, which has a lower crystallinity.

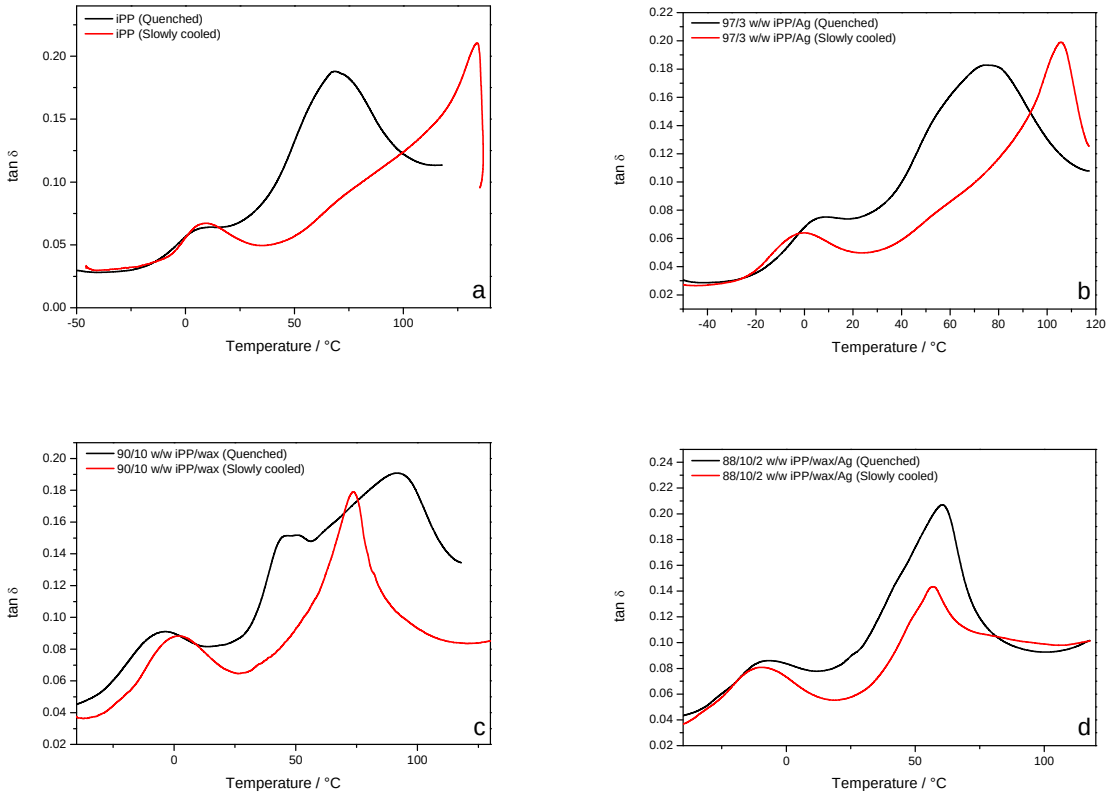

Figure 3.8 Loss factor as a function of temperature of the quenched and slowly cooled (a) iPP, (b) iPP/Ag, (c) iPP/wax and (d) iPP/wax/Ag nanocomposites

In the iPP/wax samples, the β-relaxation and wax melting peaks of the slowly cooled sample appear at a higher temperature than those of the quenched sample (Figure 3.8c). This is probably

because larger wax crystals formed during slow cooling, which had a stronger immobilizing effect on the amorphous iPP chains and which had melted at higher temperatures. There is little difference between the β-transition and wax melting temperatures of the quenched and slowly cooled samples when both wax and Ag were present (Figure 3.8d). The reason is probably that the wax crystallized mostly around the Ag nanoparticles, and since the rate at which the sample was cooled would not seriously affect the wax crystallization, and since there is very little interaction between iPP and wax, it could be expected that these transitions would not be seriously affected by the rate at which the samples were cooled.

3.4 Thermal conductivity

The thermal conductivities of the quenched and slowly cooled iPP samples increased with increasing Ag content at lower Ag contents, but leveled off at higher contents (Figure 3.9). This can be attributed to a better dispersion of the Ag particles at lower contents. At higher Ag contents the particles were not so well dispersed and formed agglomerates (Figure 3.1b). It has been reported previously that the agglomeration of filler particles increased with an increase in filler content [12-14], and that these agglomerations gave rise to lower thermal conductivities [15,16]. In the iPP/Ag nanocomposites, phonons are transported from one Ag particle to another *via* the polymer. Since the polymer is not a good thermal conductor, it is important that the filler particles must be well dispersed and fairly close to each other, and that there should be fairly strong interactive forces between iPP and Ag. In such a case heat will be transported by high frequency phonon vibrations leading to higher thermal conductivity values. However, if the particles are poorly dispersed and/or the interaction between iPP and Ag is weak, a small amount of heat will be transported by low frequency phonons as a result of higher thermal contact resistance. When the thermal conductivities of the quenched and slowly cooled samples are compared (Figure 3.9), it can be seen that the thermal conductivities of the quenched samples are significantly lower than those of the slowly cooled samples. It is known that higher crystallinities give rise to better thermal energy transport [17], which is also the reason for the better thermal conductivity of the slowly cooled samples, that have previously been shown to have much higher crystallinities (melting enthalpy values in Table 3.1).

The thermal conductivity of the quenched iPP shown in Figure 3.10 slightly increases after the addition of 10 wt% wax. This can be attributed to the wax crystals in the sample, which increased the total crystallinity (Table 3.1) and therefore the thermal energy transport. The thermal conductivity of iPP/Ag is slightly lower than that of iPP/wax, but is very similar to that of pure iPP. Again, if one looks at the values in Table 3.1, it is clear that the normalised melting enthalpy of the iPP/Ag sample is very similar within the experimental error to that of pure iPP, but lower than that of iPP/wax. As already seen, the crystallinities of the quenched samples are significantly lower, and therefore the Ag particles are probably dispersed in the amorphous phase of iPP with less contact with the crystallites, which could inhibit the thermal transport through the iPP/Ag samples. Although Ag is thermally more conductive than wax and iPP, it seems as if the thermal conductivity of the quenched iPP sample depends more on the crystallinity than on the presence of conductive metal particles. When both wax and Ag are present, the thermal conductivity of the sample is higher than that of iPP/Ag. This can again be attributed to the higher crystallinity of the sample (Table 3.1), but also to the dispersion of Ag within the highly crystalline wax phase (section 3.1). Therefore, the wax-covered Ag particles significantly increased the thermal conductivity of the quenched iPP sample.

In the slowly cooled samples (Figure 3.10), the thermal conductivity of iPP/wax is observably higher than that of iPP, which is also the result of the presence of the more crystalline wax. The thermal conductivity of the iPP/Ag sample is significantly higher than those of the pure iPP and the iPP/wax samples. According to Table 3.1, the slowly cooled iPP/Ag sample has a much higher crystallinity than the quenched sample, and therefore the Ag particles should have better contact with the iPP crystallites, which probably is the reason for the improved thermal energy transport in the slowly cooled iPP/Ag sample. The thermal conductivity of the iPP/wax/Ag sample is about the same as that of the iPP/Ag sample. In the slowly cooled iPP/Ag sample, Ag particles acts as nucleation centers and are therefore in intimate contact with the iPP crystallites. However, when wax is present, the Ag particles are no longer in contact with the iPP crystallites, but are probably covered by the crystalline wax, which will also improve the thermal energy transport. Crystallites in contact with the Ag nanoparticles, whether they are iPP or wax crystallites, seem to have a very strong influence on the thermal conductivities of the nanocomposites.

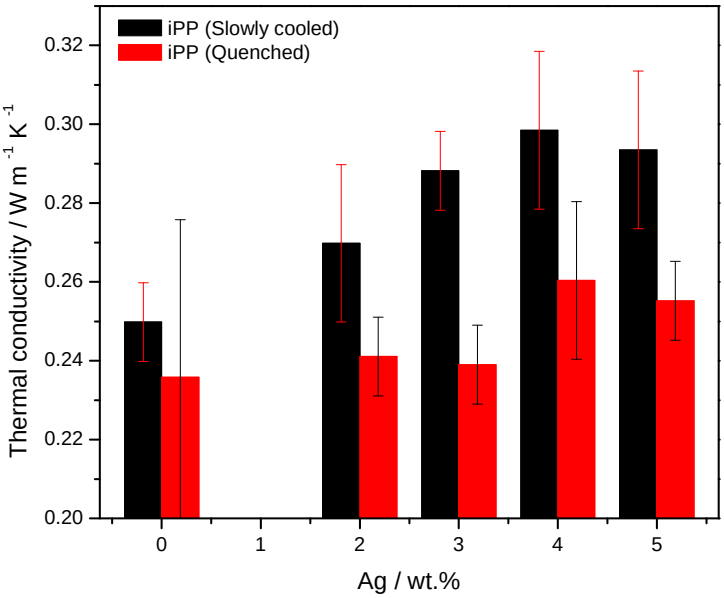

Figure 3.9 Thermal conductivities of iPP and iPP/Ag

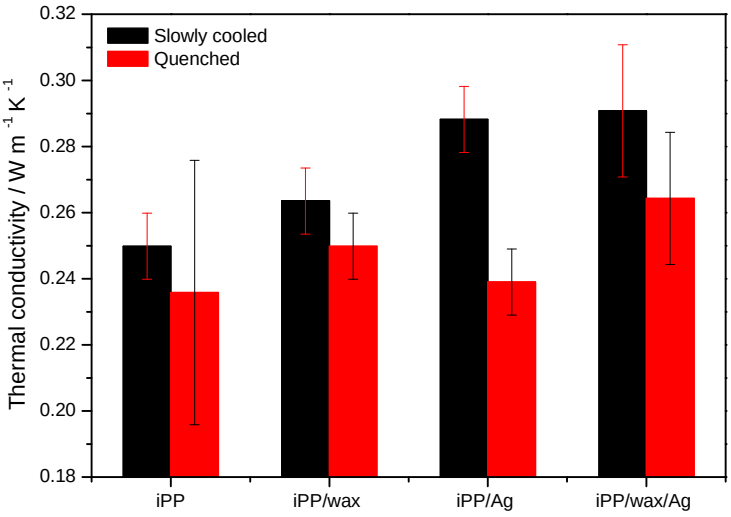

Figure 3.10 Thermal conductivities of iPP, 90/10 w/w iPP/wax, 97/3 w/w iPP/Ag and 87/10/3 w/w iPP/wax/Ag

There is no specific trend in the thermal conductivities of the quenched and slowly cooled iPP/wax/Ag samples shown in Figure 3.11. In this case there is a complex combination of effects that will influence the thermal conductivities of the samples: (1) Ag dispersion; (2) extent of agglomeration; (3) covering of Ag particles by crystalline wax; (4) extent of formation and dispersion of wax crystals in between the iPP spherulites. If the filler particles are not well dispersed, and if there are fewer (iPP or wax) crystallites, high frequency phonon movement will be inhibited and the thermal conductivity will be lower. The separate crystallization of the wax in the areas between the iPP spherulites and the covering of the Ag particles by the crystalline wax should improve the thermal conductivity, but the weak interaction between iPP and wax may negatively influence the thermal conductivity. All these factors will contribute in one way or the other to the thermal conductivity, but it is difficult to isolate any one of these factors as possible reason(s) for the differences in the conductivity. However, when the thermal conductivities of the slowly cooled and quenched samples are compared, it is clear that slowly cooled samples have higher thermal conductivities than the quenched samples because of their higher crystallinities.

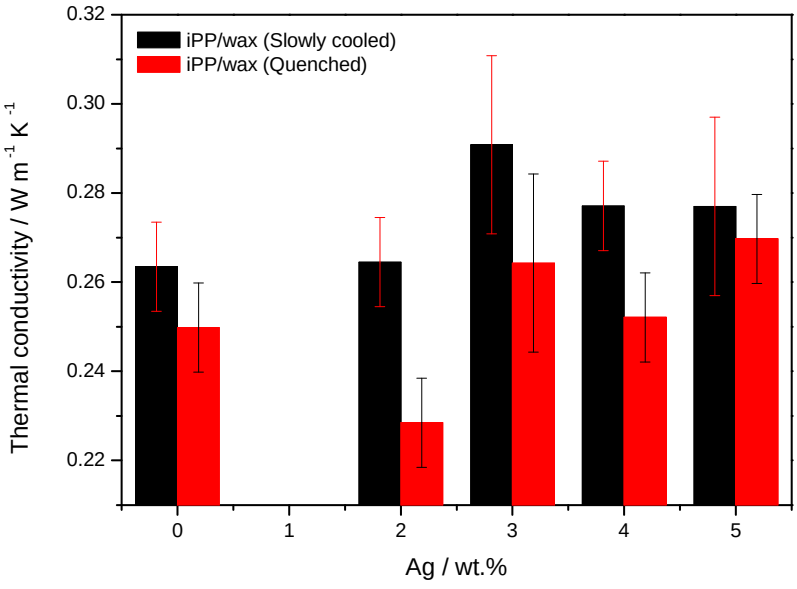

Figure 3.11 Thermal conductivity of iPP/wax and iPP/Ag with 10 wt% wax

3.5 Dielectric properties

Figure 3.12 presents the DC conductivity, conductance and susceptance of the 10 wt% wax containing iPP/Ag nanocomposites. The DC conductivity of the iPP/wax/Ag samples showed little change up to 3 wt% Ag, but increased significantly at higher Ag contents. For the lower filler content, the mean distance between the individual metal particles and aggregates must have been too large and the conductivity was therefore controlled by the insulating polymer matrix. When the distances between individual filler particles are large, electrons do not easily hop from particle to particle. However, at higher Ag contents the individual particles and aggregates were closer to each other and the mean distance between the metal particles was small enough for the electrons to fairly easily hop from one particle to another. The conductance at different frequencies showed similar behaviour (Figure 3.12a), but susceptance only showed small changes with increasing Ag content (Figure 3.12b). This is probably because the Ag particles do not improve the polarity of the blend. Both the conductance and susceptance increased with increasing frequency for all the investigated Ag concentrations, which indicates that the Ag particles did not form a well-developed conductive network. However, if one looks at the DC conductivity of the 10 wt% wax containing iPP/Ag samples, it seems as if the percolation threshold occurred at about 3.5 wt% Ag.

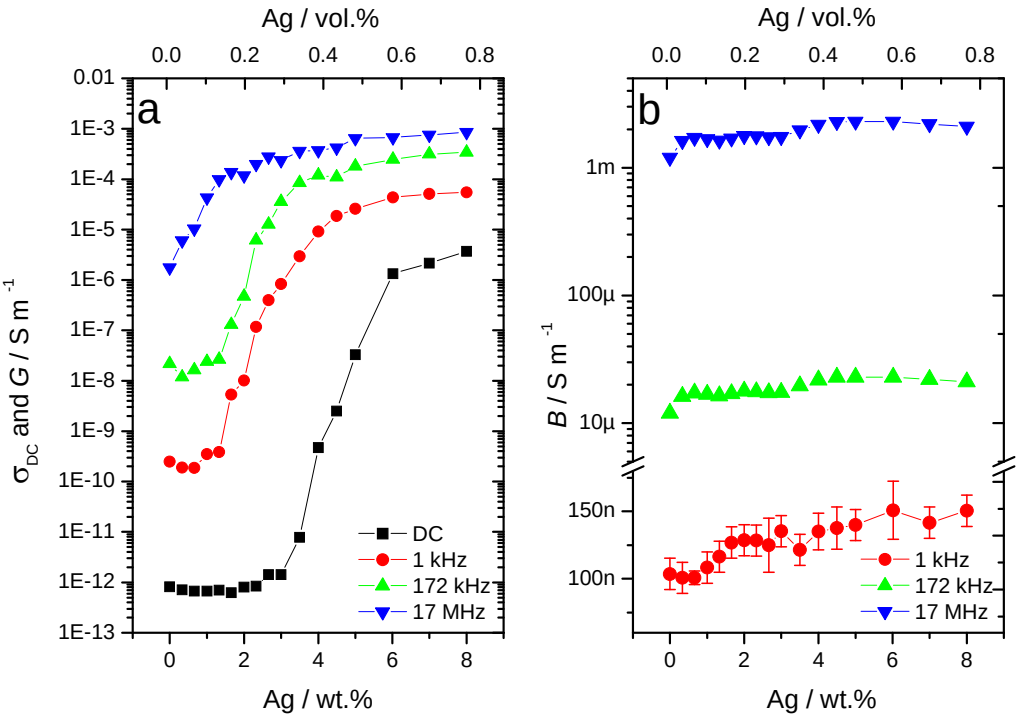

Figure 3.12 (a) DC conductivity and conductance, and (b) susceptance of 10 wt% wax containing iPP/Ag composites as function of Ag content

Figure 3.13 presents the temperature dependence of the dielectric properties of iPP and iPP/wax composites with 2 wt% Ag nanoparticles at a frequency of 172 kHz. The conductance of the samples decreased after the addition of 10 wt% wax, which can be attributed to the presence of the interface between the immiscible wax and iPP. When Ag particles are present, the conductance of the iPP/Ag sample is higher than those of pure iPP and the iPP/wax sample. In the iPP/Ag sample, the Ag particles acted as nucleation centers, as discussed in section 3.1, and are therefore in intimate contact with the iPP crystallites. The iPP crystallites in contact with the Ag particles seem to have a strong influence on the conductivity of the nanocomposites. In the presence of both wax and Ag, the conductance of iPP in the iPP/wax/Ag sample is even higher. When wax is present in the iPP/Ag sample, the Ag particles are no longer in contact with iPP crystals, but covered by the more crystalline wax which further improves the electrical conductivity. The conductance of iPP and iPP/Ag remained nearly constant at lower

temperatures, but slowly increased at higher temperatures. When wax was present, the conductance of iPP/wax and iPP/wax/Ag also remained nearly constant at lower temperatures, but decreased at about 325 K, followed by a significant increase in conductivity. This indicates that the presence of the more crystalline wax had a strong influence on the conductivity.

The susceptance showed different behaviour from that of the conductance in the presence of wax (Figure 3.13b).The susceptance of iPP/wax is higher than those of both pure iPP and iPP/Ag samples. In iPP/wax, both iPP and wax are non-polar materials, but excellent electric insulators that can be polarized by the applied electric field [18,19]. When the electric field is applied to iPP/wax, the electrons do not move through the blend as they would have done in a conductor, but move only slightly causing a small dielectric polarization so that wax more easily responded to polarization than iPP. When both wax and Ag were present, the susceptance of iPP in iPP/wax/Ag sample was higher than those of iPP/Ag and iPP/wax. This shows that in the presence of both the conductor and wax, when the external electric field was applied, the electrons moved in such a way that they were free to polarize the conductor. The wax-covered Ag particles easily responded to the polarization, and the susceptance was therefore very large. When the susceptance of iPP/wax and iPP/wax/Ag are compared, the wax slightly improved the polarity of iPP, but the wax-covered Ag particles significantly improved its polarity. The susceptance is the ratio of polarization to the applied electric field, and the changes observed in the susceptance of the composites are the result of the changes in polarization.

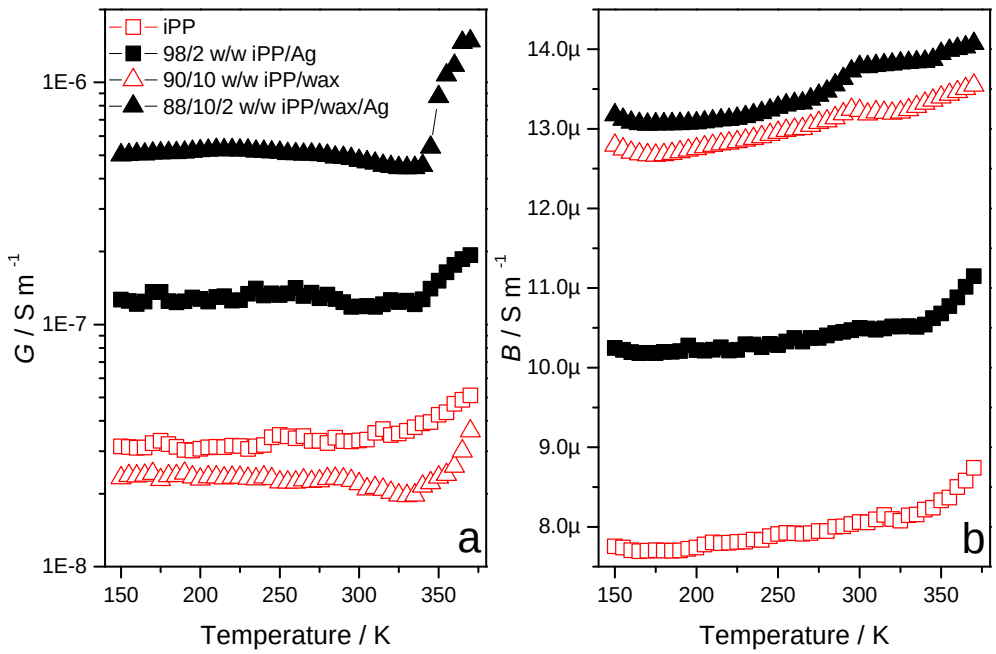

Figure 3.13 Temperature dependence of the dielectric properties of the composites with 2 wt% Ag nanoparticles at 172 kHz

In order to study the effect of Ag particles on the conductivity of iPP and the iPP/wax blend, the relative increase in admittance ($\Delta Y(f,T) = 100\cdot(Y_{pol+Ag} - Y_{pol})/Y_{pol}$) of iPP and iPP/wax due to the presence of 2 wt% Ag was determined. The results are presented in Figures 3.14 and 3.15. A transition which is associated with the γ-relaxation appeared at about 173 K in both composites. It has been previously reported that the γ-relaxation of iPP appears between 150 and 230 K, and this relaxation is usually associated with the local motions in the amorphous phase [20]. The difference in conductivity between iPP and iPP/Ag slightly increases with increasing temperature up to this temperature, followed by a decrease at higher temperatures. The non-polar iPP usually shows a γ-relaxation, but the introduction of polar groups had previously made the γ-relaxation peak disappear [19]. The observed γ-relaxation in iPP/Ag therefore confirms that the Ag particles did not improve the polarity of iPP. The iPP/wax/Ag sample has two transitions associated with the γ-transition and the softening of wax, respectively at about 173 K and 300 K (Figure 3.15). Although the conductivity of iPP/wax and iPP/wax/Ag increased with increasing temperature (Figure 3.13), the difference in their admittance increased up to the γ-transition of iPP, followed

by a decrease in conductivity at temperatures above the γ-transition. Again, the difference in conductivity (Δ*Y*) slightly increased with increasing temperature up to the onset of wax softening, followed by a significant increase in conductivity up to wax melting. At temperatures above the melting of wax the conductivity of iPP/wax/Ag more slowly increased than that of iPP/Ag, probably because of the destruction of the semi-conductive paths during the softening of the wax. The difference in conductivity only slightly changed during the softening of iPP, but significantly changed during the softening of the wax, which confirms that the Ag particles were mostly dispersed in the wax phase.

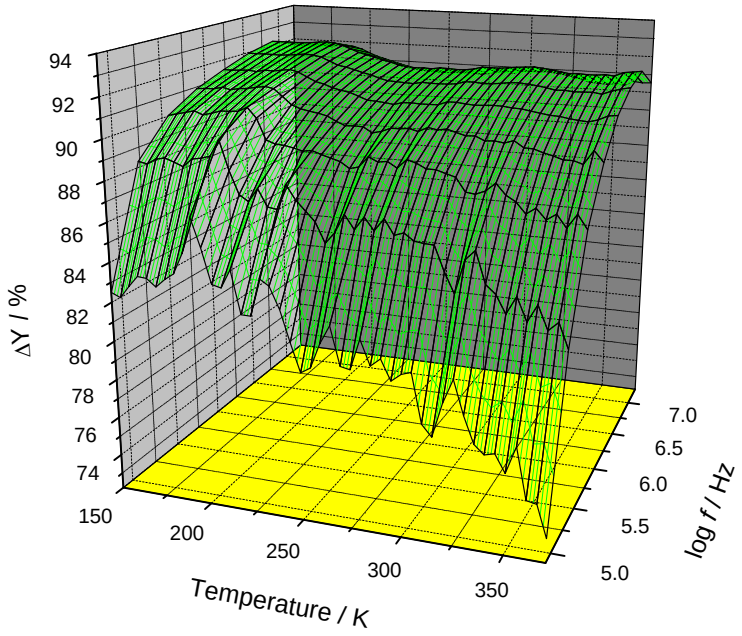

Figure 3.14 Relative increase of admittance due to the presence of 2 wt% Ag nanoparticles in iPP as function of temperature and frequency

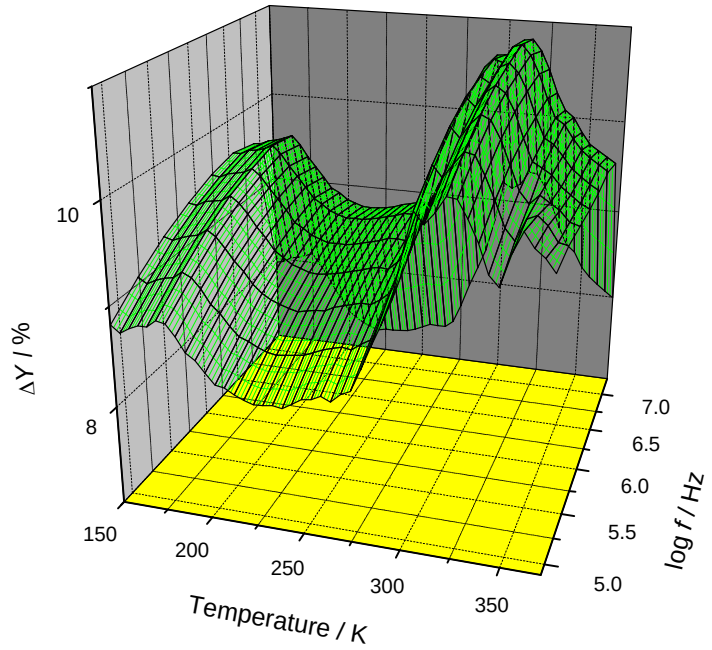

Figure 3.15 Relative increase in admittance due to the presence of 2 wt% Ag nanoparticles in 90/10 w/w iPP/wax as function of temperature and frequency

3.6 References

[1] M.L. Di Lorenzo. Spherulite growth rates in binary polymer blends. Progress in Polymer Science 2003; 28:663-689.
DOI: 10.1016/S0079-6700(02)00035-7

[2] I. Krupa, G. Miková, A.S. Luyt. Polypropylene as a potential matrix for the creation of shape stabilized phase change materials. European Polymer Journal 2007; 43:895-907.
DOI: 10.1016/j.eurpolymj.2006.12.019

[3] I. Krupa, A.S. Luyt. Thermal properties of polypropylene/wax blends. Thermochimica Acta 2001; 372:137-141.
DOI: 10.1016/s0040-6031(01)00450-6

[4] I. Krupa, G. Miková, A.S. Luyt. Phase change materials based on low-density polyethylene/paraffin wax blends. European Polymer Journal 2007; 43:4695-4705.
DOI: 10.1016/j.eurpolymj.2007.08.022.

[5] J.D. Menczel, R.B. Prime. Thermal Analysis of Polymers. Fundamentals and Applications. John Wiley & Sons, New Jersey (2009).

[6] R.J. Young, P.A. Lovell. Introduction to Polymers.CRC Press, New York (2011).

[7] H.A. Khonakdar, U. Wagenknecht, S.H. Jafari, R. Hassler, H. Eslami. Dynamic mechanical properties and morphology of polyethylene/ethylene vinyl acetate copolymer blends. Advances in Polymer Technology 2004; 23:307-315.
DOI: 10.1002/adv.20019

[8] C. Pandis, E. Logakis, A. Kyritsis, P. Pissis, V.V. Vodnik, E. Dzunuzovic, J.M. Nedeljkovic, V. Djokovic, J.C.R. Hernandez, J.L.G. Ribelles. Glass transition and polymer dynamics in silver/poly(methyl methacrylate) nanocomposites. European Polymer Journal 2011; 47:1514-1525.
DOI: 10.1016/j.eurpolymj.2011.0.06.001

[9] R.O. Sirotkin, N.W. Brooks. The dynamic mechanical relaxation behaviour of polyethylene copolymers cast from solution. Polymer 2001; 42:9801-9808.
DOI: 10.106/S0032-3861(01)00535-3

[10] M.A. Milani, D. González, R. Quijada, N.R.S. Basso, M.L. Cerrada, D.S. Azambuja, G.B. Galland. Polypropylene/graphenenanosheet nanocomposites by *in situ* polymerization: Synthesis, characterization and fundamental properties. Composites Science and Technology 2013; 84:1-7.
DOI: 10.1016/j.composcitech.2013.05.001

[11] M. Du, B. Guo, X. Cai, X. Jia, M. Liu, D. Jia. Morphology and properties of halloysite nanotubes reinforced polypropylene nanocomposites. e-Polymers 2008; 1:1490-1503.
DOI: 10.1515/epoly.2008.8.8.1490

[12] K. Chrissafis, K.M. Paraskevopoulos, S.Y. Stavrev, A. Docoslis, A. Vassiliou, D.N. Bikiaris. Characterization and thermal degradation mechanism of isotactic polypropylene/carbon black nanocomposites. Thermochimica Acta 2007; 465:6-17.
DOI: 10.1016/j.tca.2007.08.007

[13] V. Vladimirov, C. Betchev, A. Vassiliou, G. Papageorgiou, D. Bikiaris. Dynamic mechanical and morphological studies of isotactic polypropylene/fumed silica nanocomposites with enhanced gas barrier properties. Composites Science and Technology 2006; 66:2935-2944.

DOI: 10.1016/j.compscitech.2006.02.010

[14] A. Vassiliou, D. Bikiaris, K. Chrissafis, K.M. Paraskevopoulos, S.Y. Stavrev, A. Docoslis. Nanocomposites of isotactic polypropylene with carbon nanoparticles exhibiting enhanced stiffness, thermal stability and gas barrier properties. Composites Science and Technology 2008; 68:933-943.
DOI: 10.1016/j.compscitech.2007.08.019

[15] Y.S. Song, J.R. Youn. Influence of dispersion states of carbon nanotubes on physical properties of epoxy nanocomposites. Carbon 2005; 43:1378-1385.
DOI: 10.1016/j.carbon.2005.01.007

[16] K. Yang, M. Gu. Enhanced thermal conductivity of epoxy nanocomposites filled with hybrid filler system of triethylenetetramine-functionalized multi-walled carbon nanotube/silane-modified nano-sized silicon carbide. Composites Part A 2010; 41:215-221.
DOI: 10.1016/j.compositesa.2009.10.019

[17] I. Krupa, I. Novák I. Chodák. Electrically and thermally conductive polyethylene/graphite composites and their mechanical properties. Synthetic Metals 2004; 145:245-252.
DOI: 10.1016/j.synthmet.2004.05.007

[18] I. Krupa, A.S. Luyt. Thermal properties of uncross-linked and cross-linked LLDPE/wax blends. Polymer Degradation and Stability 2000; 70:111-117.
DOI: 10.1016/S0141-3910(00)00097-5

[19] E. Suljovrujic. Complete relaxation map of polypropylene: Radiation-induced modification as dielectric probe. Polymer Bulletin 2012; 68:2033-2047.
DOI: 10.1007/s00289-012-0714-1

[20] E. Suljovrujic, S. Trifunovic, D. Milicevic. The influence of gamma radiation on the dielectric relaxation behavior of isotactic polypropylene: The α relaxation. Polymer Degradation and Stability 2010; 95:164-171.
DOI: 10.1016/j.polymdegradstab.200911.034

CHAPTER 4

Conclusions

The purpose of the study was to correlate the morphologies of quenched and slowly cooled iPP/Ag and iPP/wax/Ag samples with the thermal and thermomechanical properties, as well as the thermal and electrical conductivities. The Ag nanoparticles were concentrated at the growth centres of the iPP spherulites in the iPP/Ag nanocomposites and formed nucleation centres for the crystallization of iPP. Wax crystallized separately from iPP in the areas between the spherulites in the iPP/wax/Ag nanocomposites, and influenced the growth of the iPP spherulites by acting as a plasticizer or diluent. The Ag nanoparticles had a larger affinity for wax and were no longer observed at the growth centres of the iPP spherulites, but remained in the wax phase which was dispersed in between the iPP spherulites. The Ag nanoparticles, whether in the iPP spherulites or in the wax phase, had little influence on the mobility of the iPP chains and on its crystallinity. The wax-covered Ag particles more significantly improved the thermal and electrical conductivities of the samples than the Ag particles in neat iPP. The Ag particles in iPP/Ag had little influence on the modulus of iPP, but the presence of both wax and Ag particles significantly reduced the modulus, probably because of the plasticizing effect of the wax.

With increasing Ag contents in iPP/Ag, the nanoparticles remained at growth centres of the iPP spherulites, but the filler was not so well dispersed and the extent of the agglomeration increased. In iPP/wax/Ag with higher filler contents, Ag agglomerates were also observed at the growth centres of the iPP spherulites, probably because the wax content was too low for all the particles to be covered by wax. The Ag particles had little influence on the crystallinites of iPP in all the samples, even at the higher contents. The thermal conductivities of both the iPP and iPP/wax based samples increased with increasing Ag content, but leveled off at higher filler contents, while the electrical conductivities continued increasing with increasing filler contents.

In iPP/wax blend the melting enthalpies of iPP increased with an increase in wax content, which could only be attributed to co-crystallization between the wax and iPP. The highly crystalline wax increased the stiffness of the quenched samples because of the lower iPP crystallinity, but it

had a softening effect on the slowly cooled samples because of the higher iPP crystallinity and the plasticizing effect of the wax. The presence of wax increased the thermal conductivities, probably because of its higher crystallinity, but decreased the electrical conductivities of the blends.

Both the quenching and slow cooling treatments had an influence on the crystallinities of the samples. Because of their lower crystallinities, the thermal conductivities of the quenched samples were significantly lower than those of the slowly cooled samples. The slowly cooled iPP and iPP/Ag samples showed higher moduli than the quenched samples because of their higher crystallinities. In the iPP/wax blend, the differences in the iPP crystallinities of the quenched and slowly cooled samples had less influence on the modulus of the samples because of the presence of highly crystalline wax. When both wax and Ag were present, the slowly cooled sample showed a lower modulus than the quenched sample, indicating that the wax-covered Ag particles provided more stiffness in the quenched sample.

In conclusion, the highly crystalline wax improved the thermal heat transport of both the quenched and slowly cooled samples, but decreased the electrical conductivity because of the immiscibility of iPP and wax. The presence of Ag in the iPP/wax phase blend significantly improved the thermal and electrical conductivities of both the quenched and slowly cooled samples, because of the coverage of the Ag particles by the highly crystalline wax.

Based on our findings, there are some areas that need further investigation. These are the investigation of the dispersion of Ag particles in quenched iPP and iPP/wax blends, the influence of quenching and slow cooling treatments on the electrical conductivity of the nanocomposites, and the influence of wax on the percolation threshold of both the quenched and slowly cooled iPP/Ag nanocomposites.

ACKNOWLEDGEMENTS

Firstly, I would like to thank the Almighty God for giving me strength and courage for writing this thesis.

I would like to thank **Prof. Adriaan Stephanus Luyt and Dr. Dudić Dusko**, for their supervision, guidance, encouragement and patience especially during the hard times in this project.

I would like to thank all my former and present colleagues in the polymer science research group (Ms. Thandi Gumede, Ms. Thollwana Makhetha, Ms. Motshabi Sibeko, Ms. Puseletso Mofokeng, Ms. Cheryl-Ann Clarke, Ms. Tshepiso Molaba, Ms. Lerato Mollo, Mr. Teboho Mokhena, Mr. Jonas Mochane, Mr. Teboho Motshweneng, Mr. Tladi Mofokeng, Dr. Thabang Mokhothu, Mr. Shale Sefadi, Mr. Mfiso Mngomezulu, Dr. Tshwafo Motaung, Mr. Tsietsi Tsotetsi, Mr. Tyson Mosoabisane, Dr. Nomampondomise Molefe, Mrs. Moipone Malimabe and Mrs. Marlize Jackson).

I would also like to thank the University of the Free State (UFS), Sasol Inzalo and the National Research Foundation (NRF) for financial support.

Lastly, I wish to give all my thanks to Thabo Phelephe for his support, my Parents (Diau Albert Molaba and Dibabatso Esther Molaba) for raising me and making me the person I am today, and my siblings (Rorisang Molaba and Mantshieng Molaba) for their encouragement and support.

Appendix A

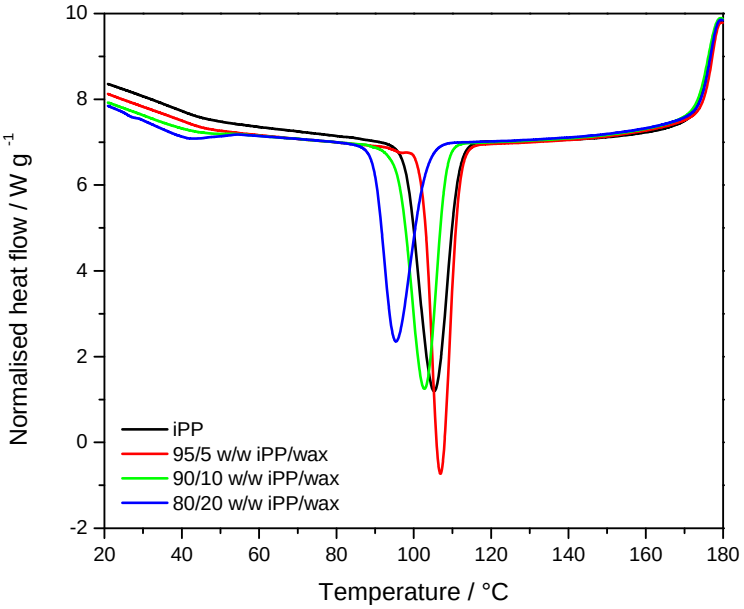

Figure A.1 DSC cooling curves of iPP and iPP/Ag nanocomposites quenched from the melt

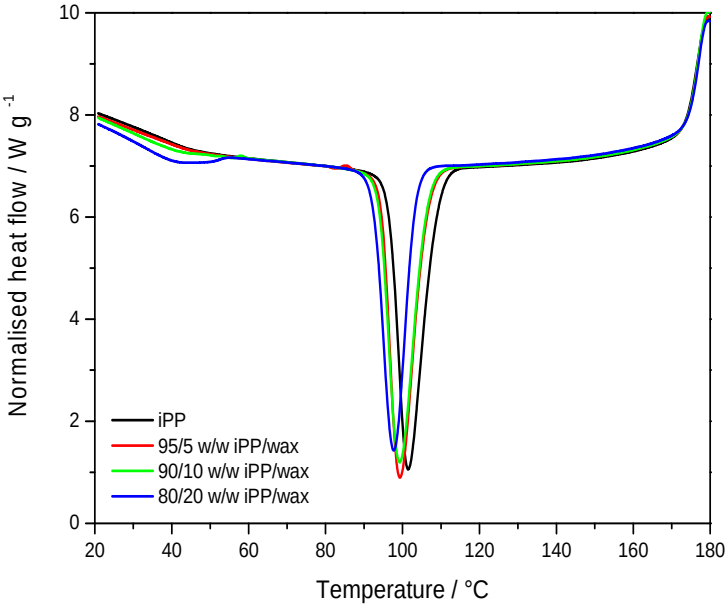

Figure A.2 DSC cooling curves of iPP and iPP/wax blends slowly cooled from the melt

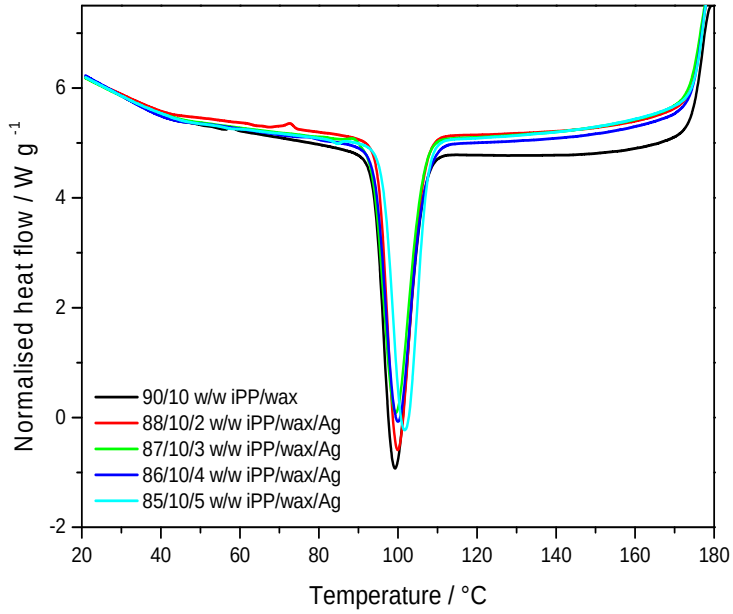

Figure A.3 DSC cooling curves of iPP/wax blends and the 10 wt% wax containing iPP/Ag nanocomposites quenched from the melt

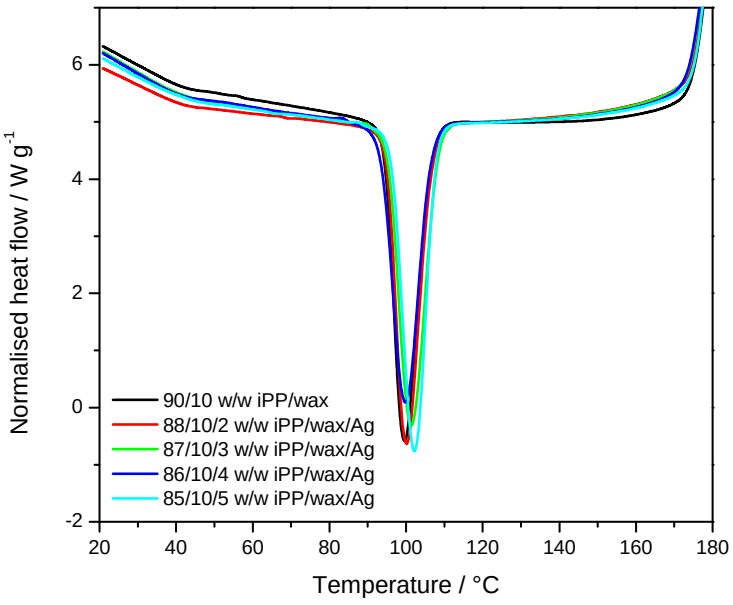

Figure A.4 DSC cooling curves of iPP/wax and the 10 wt% containing iPP/Ag nanocomposites slowly cooled from the melt

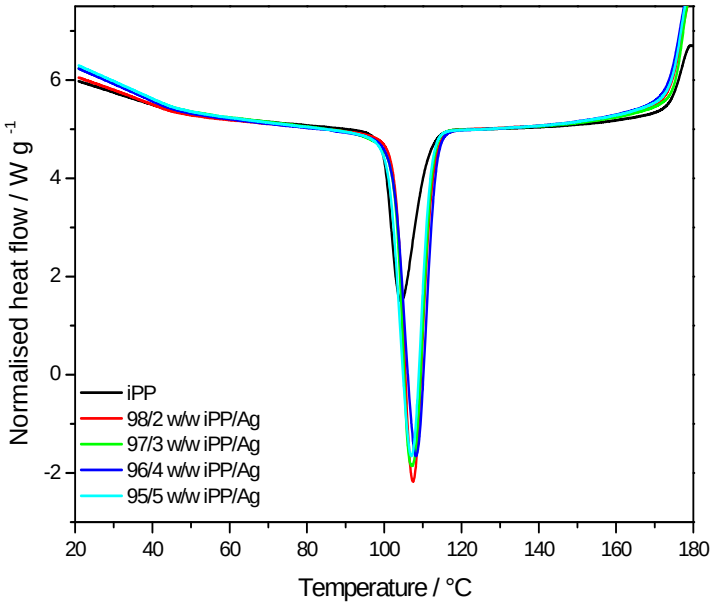

Figure A.5 DSC cooling curves of the pure iPP and iPP/Ag nanocomposites quenched from the melt

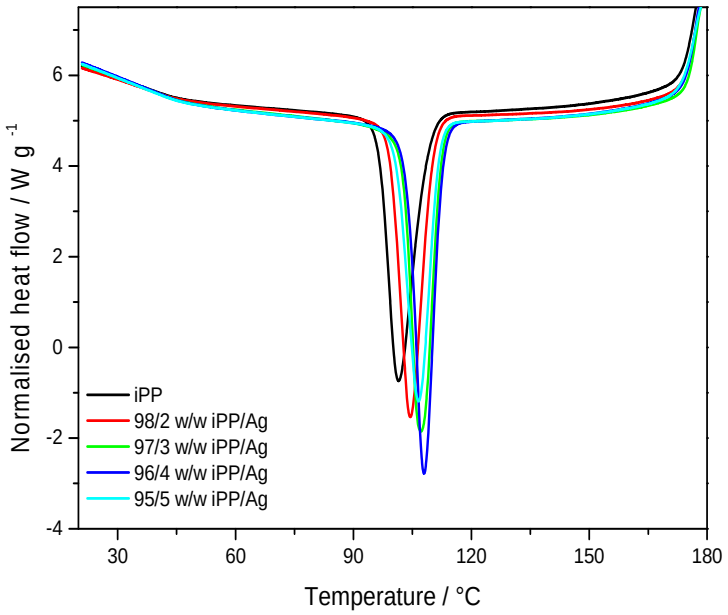

Figure A.6 DSC cooling curves of iPP and iPP/Ag nanocomposites slowly cooled from the melt

Appendix B

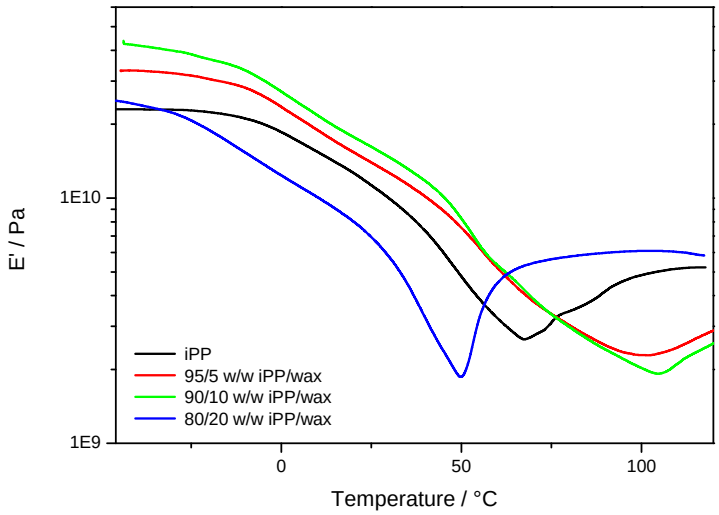

Figure B.1 Storage modulus as a function of temperature of iPP and iPP/wax quenched from the melt

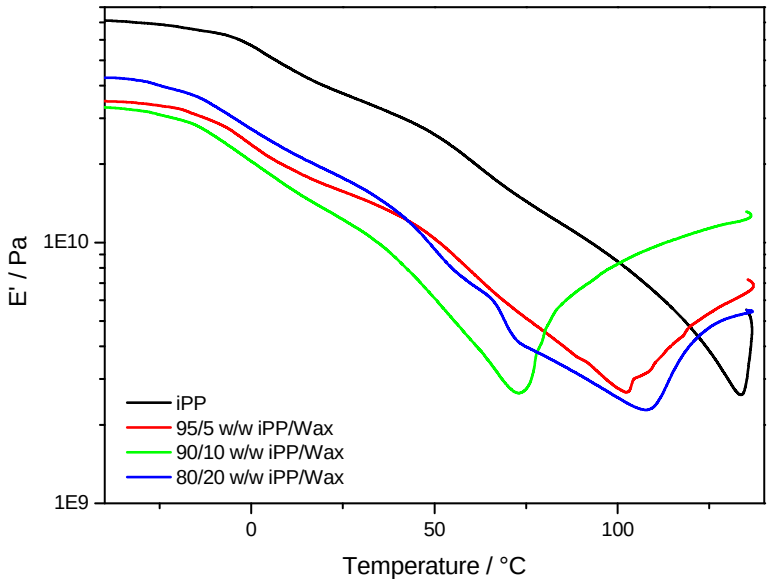

Figure B.2 Storage modulus as a function of temperature of iPP and iPP/wax slowly cooled from the melt

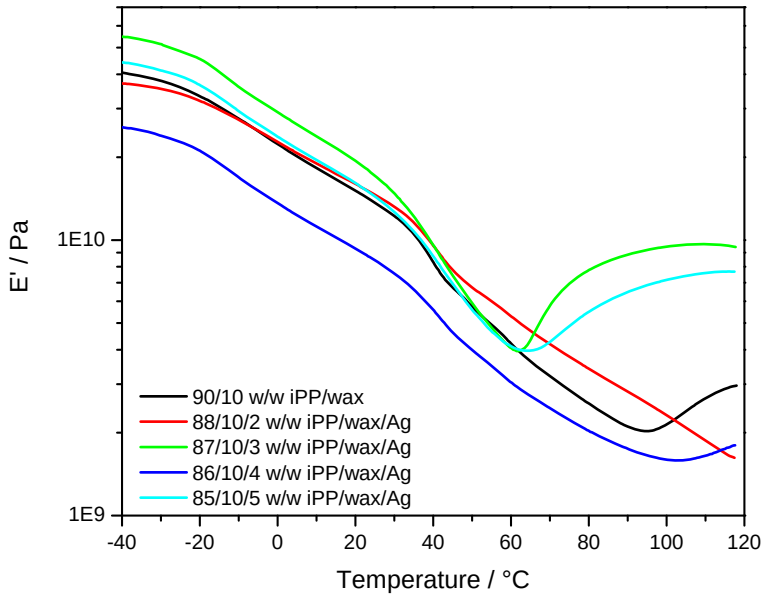

Figure B.3 Storage modulus as a function of temperature of iPP/Ag and iPP/wax/Ag quenched from the melt

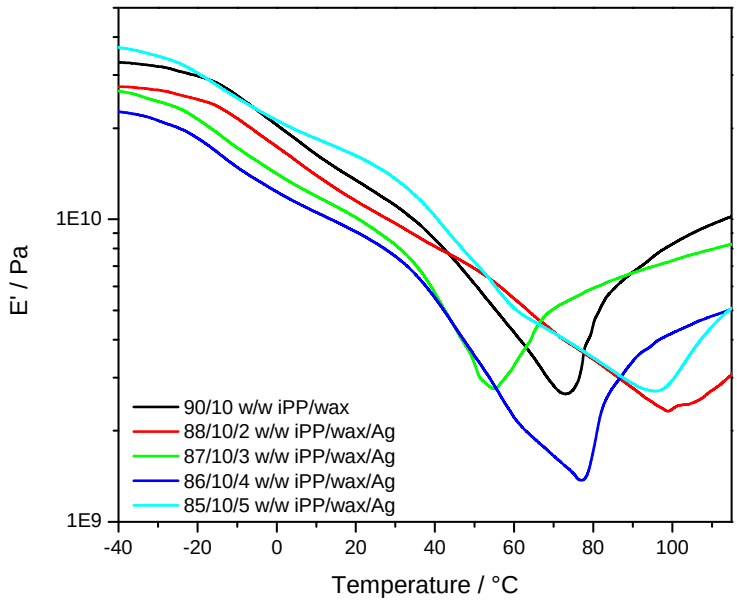

Figure B.4 Storage modulus as a function of temperature of iPP/wax and iPP/wax/Ag slowly cooled from the melt

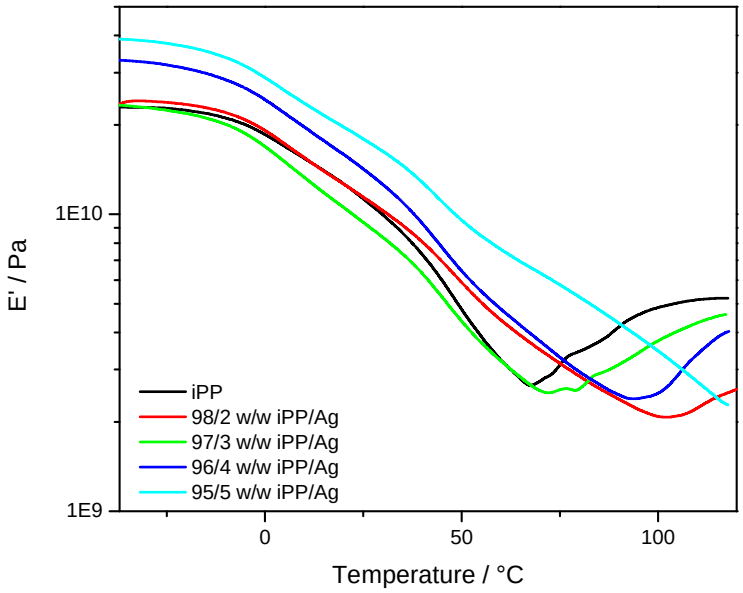

Figure B.5 Storage modulus as a function of temperature of iPP and iPP/Ag quenched from the melt

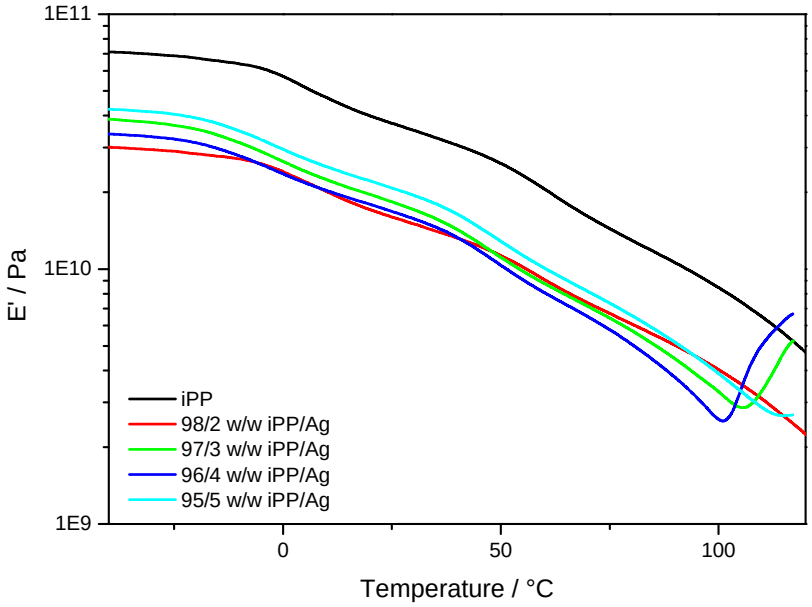

Figure B.6 Storage modulus as a function of temperature of iPP and iPP/Ag slowly cooled from the melt

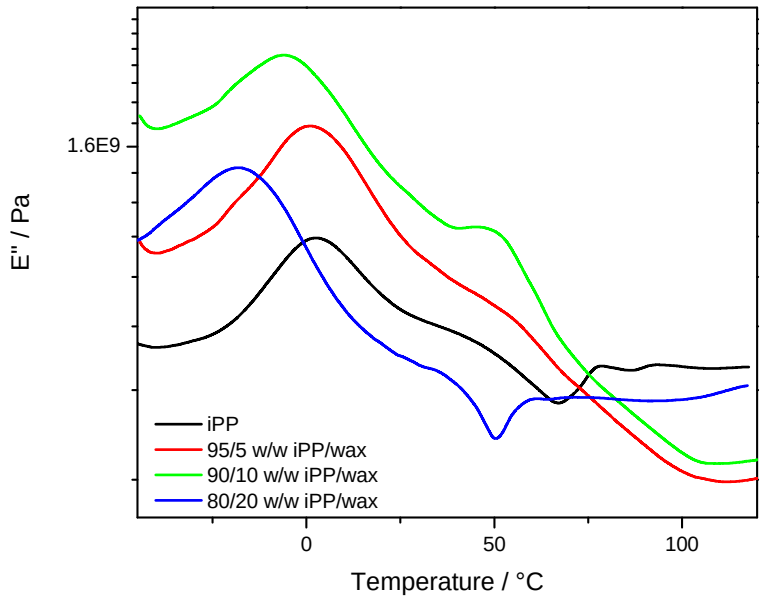

Figure B.7 Loss modulus of iPP and iPP/wax blends quenched from the melt

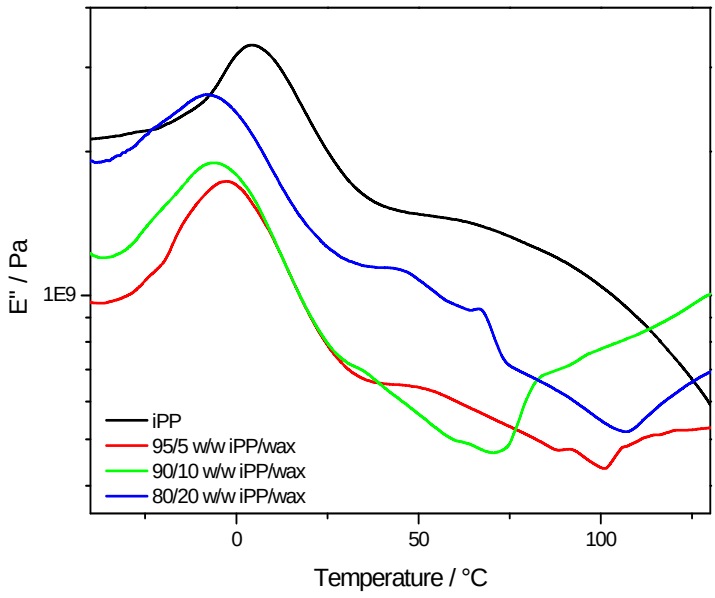

Figure B.8 Loss modulus of iPP and iPP/wax blends slowly cooled from the melt

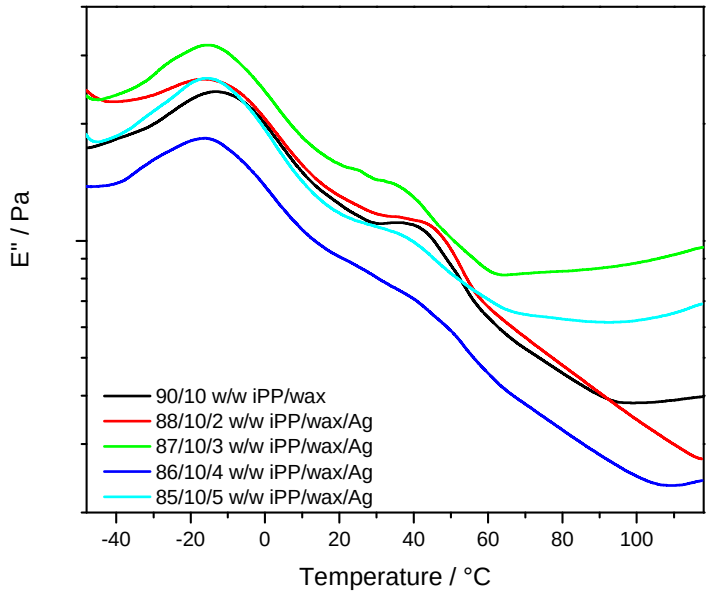

Figure B.9 Loss modulus of iPP/wax and iPP/wax/Ag blends quenched from the melt

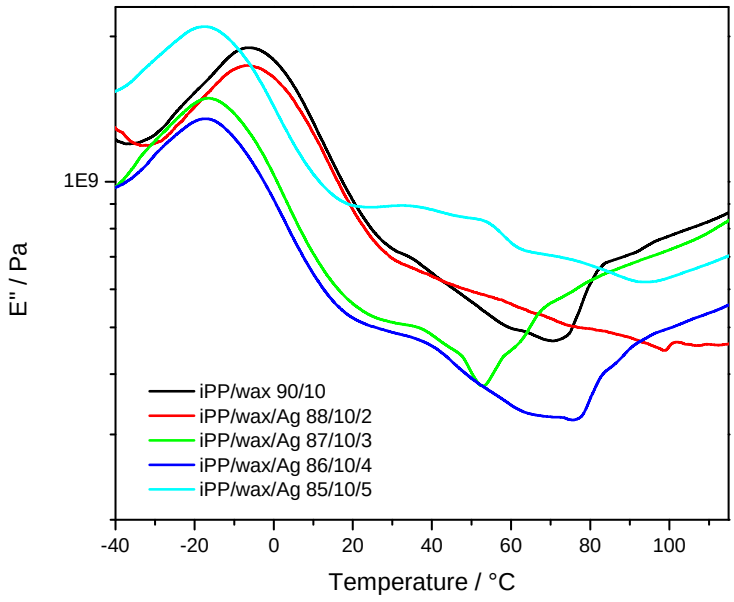

Figure B.10 Loss modulus of iPP and iPP/wax blends slowly cooled from the melt

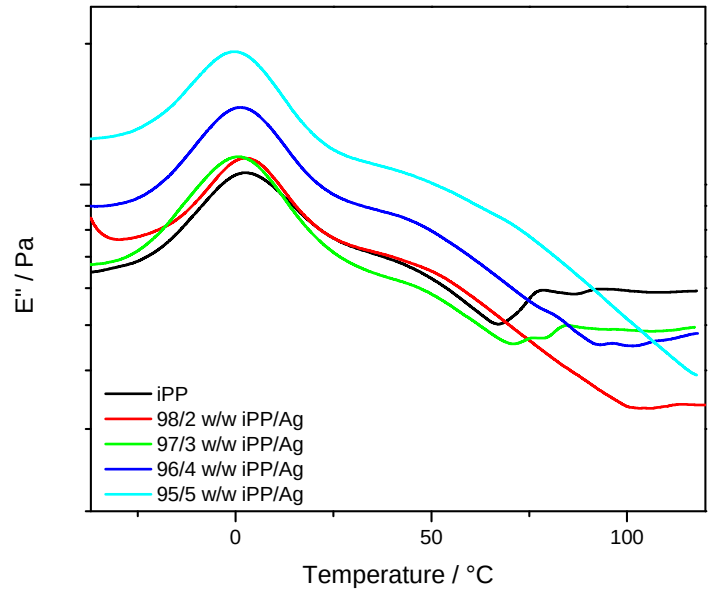

Figure B.11 Loss modulus of iPP and iPP/Ag nanocomposites quenched from the melt

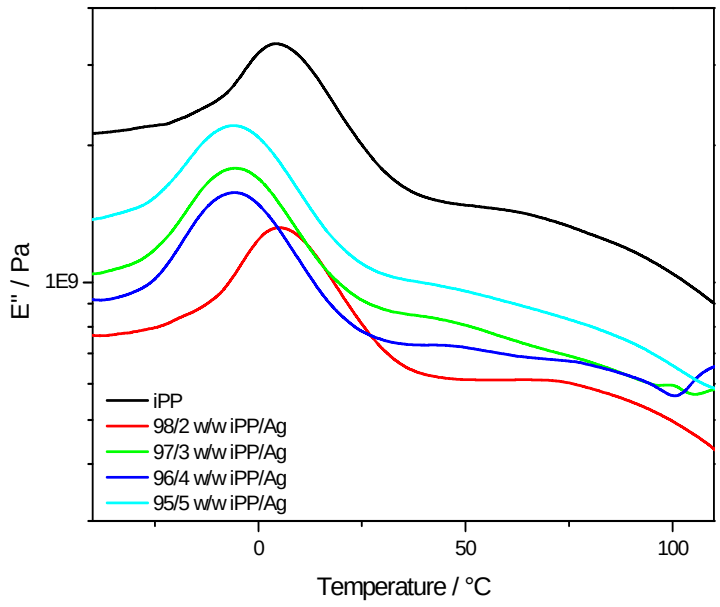

Figure B.12 Loss modulus of iPP and iPP/Ag nanocomposites slowly cooled from the melt

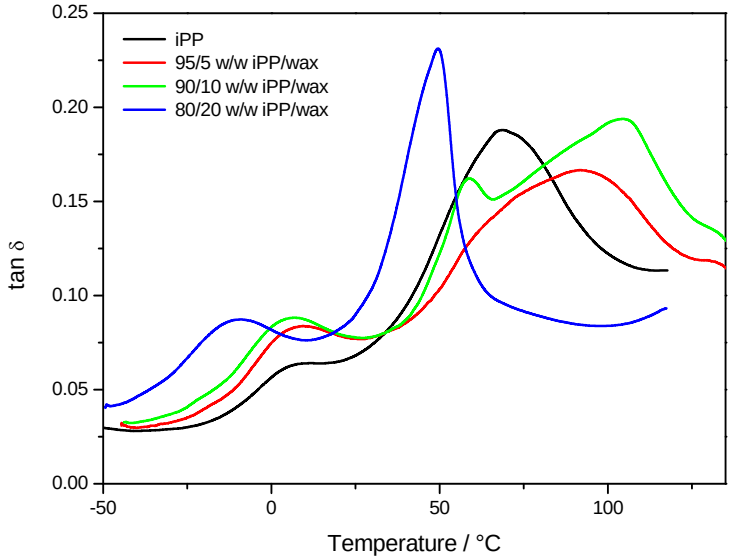

Figure B.13 Loss factor as a function of temperature of iPP and iPP/wax quenched from the melt

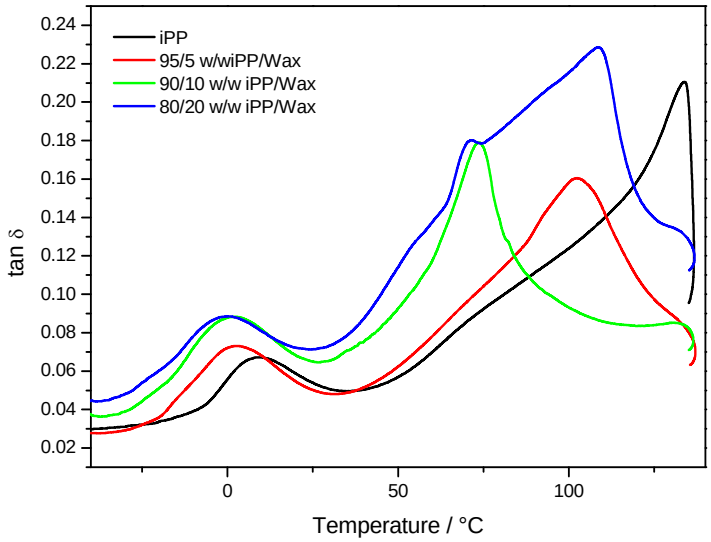

Figure B.14 Loss factor as a function of temperature of iPP and iPP/wax slowly cooled from the melt

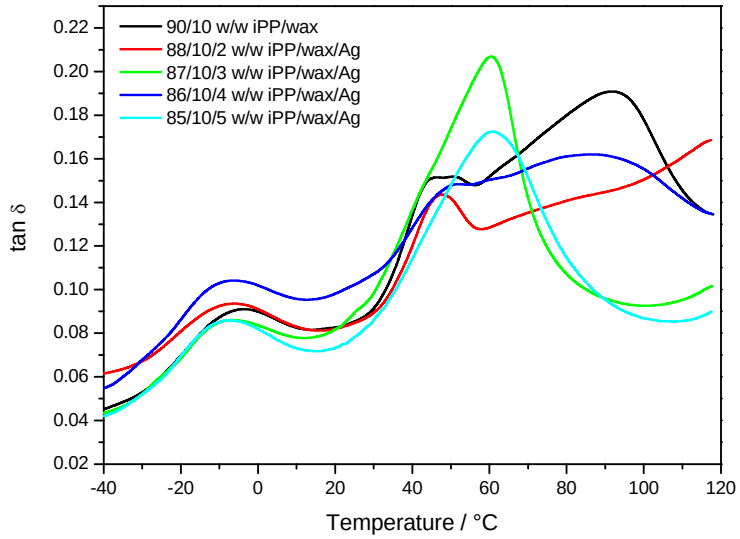

Figure B.15 Loss factor as a function of temperature of iPP/wax and iPP/wax/Ag quenched from the melt

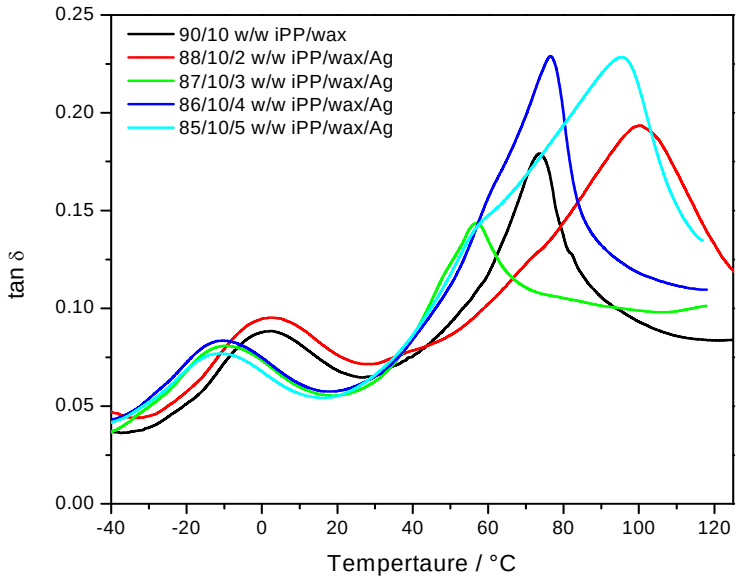

Figure B.16 Loss factor as a function of temperature of iPP/wax and iPP/wax/Ag slowly cooled from the melt

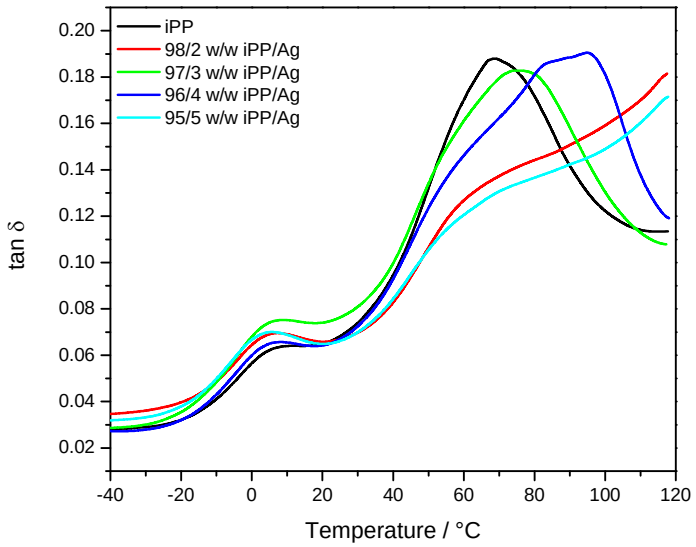

Figure B.17 Loss factor as a function of temperature of iPP and iPP/Ag quenched from the melt

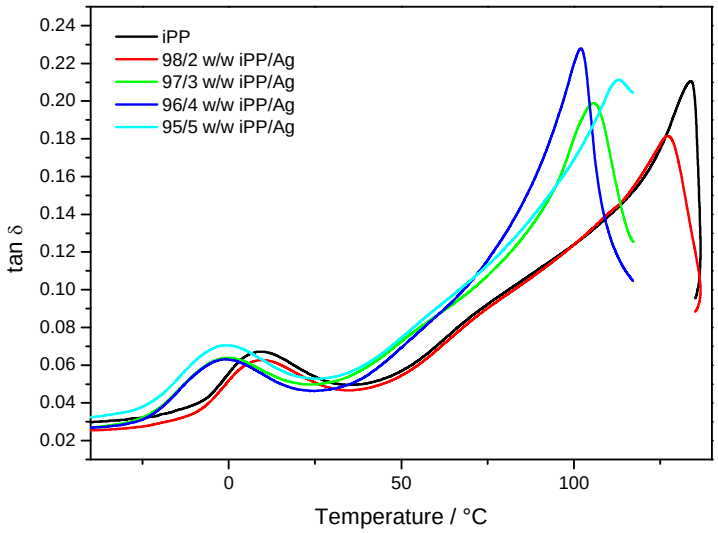

Figure B.18 Loss factor as a function of temperature of iPP and iPP/Ag slowly cooled from the melt